CHALMERS
UNIVERSITY OF TECHNOLOGY

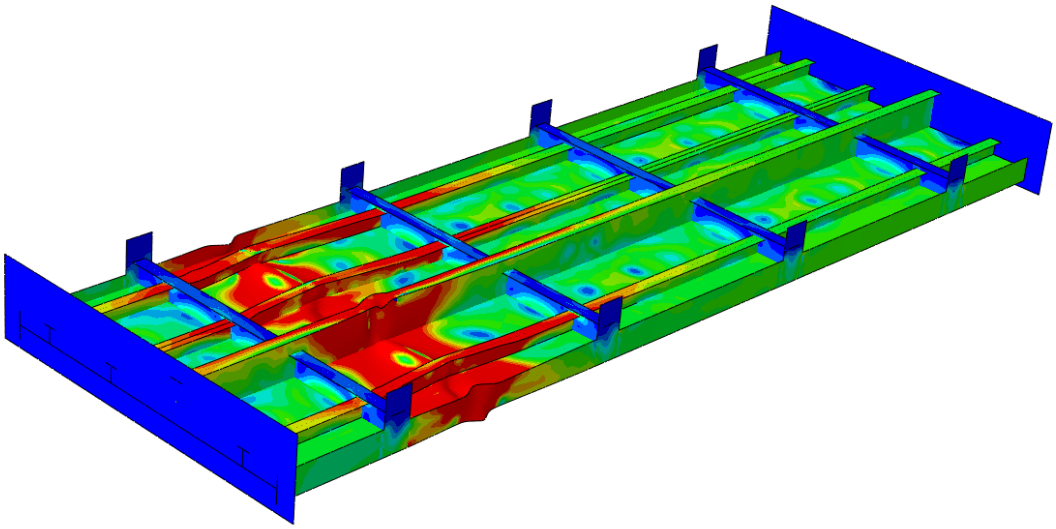

Ultimate strength analysis of stiffened plate structures

Master's thesis in the International Master's Programme in Naval Architecture and Ocean Engineering

MCANTHONY NWOYE

DEPARTMENT OF MECHANICS AND MARITIME SCIENCES
DIVISION OF MARINE TECHNOLOGY

CHALMERS UNIVERSITY OF TECHNOLOGY
Gothenburg, Sweden 2022
www.chalmers.se

MASTER'S THESIS IN THE INTERNATIONAL MASTER'S PROGRAMME
NAVAL ARCHITECTURE AND OCEAN ENGINEERING

Ultimate strength analysis of stiffened plate structures

MCANTHONY NWOYE

Department of Mechanics and Maritime Sciences
Division of Marine Technology
CHALMERS UNIVERSITY OF TECHNOLOGY
Göteborg, Sweden 2022

Ultimate strength analysis of stiffened plate structures

MCANTHONY NWOYE

Master's Thesis 2022:69
Department of Mechanics and Maritime Sciences
Division of Marine Technology
Chalmers University of Technology
SE-412 96 Göteborg
Sweden
Telephone: + 46 (0)31-772 1000

Cover:
Failure recorded for a model with uniform bottom field plate thickness of 6.35mm
Figure 4.20
Name of the printers / Department of Mechanics and Maritime Sciences
Göteborg, Sweden 2022-10-28

Ultimate strength analysis of stiffened plate structures
Master's thesis in Naval Architecture and Ocean Engineering
MCANTHONY NWOYE
Department of Mechanics and Maritime Sciences
Division of Marine Technology
Chalmers University of Technology

Abstract

An international benchmark study on which this thesis is based compared FEA results to a reference experiment. The FEA results and experiment were in agreement with respect to ultimate capacity but not for modes and location of failure. This thesis, therefore, investigates possible factors that impact ultimate capacity, failure mode and location. This was achieved analytically and by non-linear finite element analysis.

The method employed was to systematically alter the geometry used in the benchmark study and then observe the changes that influenced the results. The ultimate capacity of some of these models was also calculated by implementing existing empirical models in python. The models were then subjected to linear and non-linear buckling analysis in Abaqus. The results are presented as force–displacement curves and von Mises stress plots.

The ultimate capacity was shown to be sensitive to longitudinal stiffener configuration, longitudinal stiffener dimensions, bottom plate configuration and bottom plate thickness. The empirical estimation of ultimate capacity was shown to be quite conservative when compared to the FEA prediction. The failure location however was found to be most sensitive to the bottom plate configuration. Models with uniform bottom plate field thickness had an influence on the location of failure. Most importantly, two of the models with uniform bottom plate fields studied predicted the failure location recorded in the reference experiment. The effects of the boundary conditions and direction of force application prescribed are also documented.

Keywords: failure location, linear buckling analysis, non-linear finite element analysis, ultimate capacity.

Contents

List of figures

List of tables

Preface

The contents of this thesis are in fulfilment of the requirements for the international master's degree in Naval Architecture and Ocean Engineering at the department of Mechanics and Maritime Sciences at Chalmers University of Technology in Gothenburg, Sweden.

I would like to thank the examiner Professor Jonas W. Ringsberg for the opportunity to work on this subject and carry out research based on his previous work. Working under his tutelage kept me motivated and on several occasions helped bring me back on track.

I would also like to thank the supervisor on this thesis Artjoms Kuznecovs for his guidance, insightful questions and feedback throughout the duration of this research project. His continuous prompt feedback helped steer this project.

I am grateful for a colleague and friend Daniel Vergara whose constant encouragement played a major role for me in this project. We had interesting discussions on data processing and working in Python which challenged me to delve into and execute a portion of my thesis in Python.

I am also grateful to my parents Mr and Mrs Nwoye and my sister Dr. Thelma Nwoye for their ceaseless support both on this thesis and during my time at Chalmers.

I would be remiss not to mention officers of the Nigerian Navy Capt. GU Nwabunike, Lt. DC Okafor, S/Lt MB Lasisi, S/Lt AM Faponle, MWOMEA OM Adebiyi, POBP OL Anjorin (rtd) and the entire team at the ship design centre of the Naval Dockyard Limited. I appreciate the knowledge gained from these supervisors and collegues turned mentors and friends. I also appreciate the experiences and memories made during my time with these wonderful people.

I would also like to mention a dear friend Eline Van Der Heeg who helped me navigate a difficult time and without whom I certainly would not have seen this thesis to its completion. Thank you El.

There are still a plethora of people who I haven't mentioned here who have been sources of encouragement, I appreciate you all.

Finally, I would live to immortalize the late Rev. McDavis Ibekwe and Patrick Amaefule who were influential to the person I am today. My uncle Patrick helped keep me front sight focused during my time at Chalmers and I was blindsided by his passing in the summer of 2021. I will remember fondly the conversations we had on a broad range of subjects.

Göteborg, 2022-10-28

MCANTHONY NWOYE

Notations

a	Length of plate	[mm]
β	Plate slenderness ratio	[-]
b	Breadth of plate	[mm]
b_f	Stiffener flange breadth	[mm]
c	Coefficient of empirical formulation	[-]
E	Young's modulus	[GPa]
h_w	Stiffener web height	[mm]
I_{pz}	Moment of inertia of plate about z-axis	[-]
I_{sz}	Moment of inertia of stiffener about z-axis	[-]
λ	Column slenderness ratio	[-]
ν	Poisson's ratio	[-]
P_{cr}	Ultimate capacity	[MN]
σ_{xu}	Compressive ultimate strength	[MPa]
σ_{Yeq}	Equivalent yield stress	[MPa]
t_f	Stiffener flange thickness	[mm]
t_p	Plate thickness	[mm]
t_w	Stiffener web thickness	[mm]

1 Introduction

Shipping contributes significantly to the global economy as shown by Asariotis et al. (2018) and Stevens, (2018). Global seaborne trade experienced an increase of 411 million tons in transported volume bringing the total shipped volume to 10.7 billion tons for the year 2017; see Asariotis et al. (2018). Essential to seaborne trade and the oil industry are ships and offshore platforms. There would be no significant oil exploration nor would seaborne trade survive without offshore platforms and ships. It would therefore be beneficial to study the tools upon which these industries relevant to global trade thrive. It is therefore of significance to have an ever-evolving understanding of these structures.

Ships and offshore platforms are either in part or wholly built from stiffened plates to achieve the strength required in service. They are typically non-prismatic in shape and to calculate their longitudinal strength and hull girder response to applied loads, a prismatic portion (midship section) of the entire structure is typically considered. The configuration of plates and stiffeners that constitute large portions of these structures can be described as stiffened plate structures. It, therefore, becomes possible to understand the behaviour of these structures by studying sample stiffened plate structures. The constitutive structural elements of these structures are thin plates and stiffeners which fit the description of thin-walled structures and are therefore analyzed as such. Knowledge obtained from this analysis would provide insight into the load-bearing capacity of these structures and how they respond to static and dynamic loads.

An important parameter when investigating engineering materials and structures is the ultimate strength. Exceeding ultimate capacity results in failure and could have catastrophic consequences for ship hulls and platform structures. This has inspired research into effective means of prediction for the ultimate capacity and resultant failure modes for a given stiffened plate structure. The correct evaluation of the ultimate capacity level is used to establish an acceptable safety margin for a given structure. This is done by comparing the ultimate capacity to possible extreme applied loads.

1.1 Background and motivation

Paik & Thayamballi (2003) emphasizes that the failure of a structural member should occur in a ductile manner. This mitigates the sudden collapse of the structure and allows for the redistribution of internal stresses before global failure. The failure modes are therefore relevant in keeping track of the structural members and ensuring failure in the members does not result in an abrupt decrease of structural capacity.

According to Paik & Thayamballi (2003), structural design with emphasis on limit state design as opposed to the previous standard of allowable stress design is the current accepted practice. The formulation of a limit state attempts to predict the condition(s) that would cause failure in a structural member or the entire structure being considered. The aforementioned failure refers to the inability of a structure to perform its intended function. In structural design, four limit states are considered. They are:

a. Serviceability limit state
b. Ultimate limit state
c. Accidental limit state
d. Fatigue limit state

For the purpose of this thesis, the ultimate limit state (ULS) is of primary concern and would form the basis of the papers subsequently reviewed. The ULS is concerned with the rigidity and strength of a structure and represents structural collapse due to a critical loss of stiffness and strength; see Paik & Thayamballi (2003). A reference stiffened plate structure has been analyzed in an international benchmark study presented in Ringsberg et al. (2021). This thesis intends to further investigate and attempt to corroborate the findings of the benchmark study.

The international benchmark study aimed to investigate existing class rules and guidelines for ultimate capacity prediction and how they compare to each other. It also assessed the influence of participant modelling and simulation methods on buckling collapse and ultimate capacity prediction. The study physically constructed the stiffened plate structure and subjected it to in-plane compressive loads to establish the ultimate capacity and buckling collapse behaviour of the structure. Participants of the study then modelled the same structure in commercial FEA software and the results from the FEAs were compared to those obtained from physical testing. Some participants also utilized numerical code for the prediction of ultimate capacity in the first two phases and presented the results along with FEA results. The ultimate capacity obtained from FEA was slightly underestimated but maintained a good agreement with those obtained from the physical test. All predictions, however, underestimated the displacement at ultimate capacity (critical displacement) and failed to capture the failure modes and location. The study documents the effects of geometric imperfections and residual stresses on the resulting ultimate capacity, failure modes and location in FEA. It was noted that the geometric imperfections, distortions and residual stresses are essential for the correct prediction of ultimate capacity, failure modes and location.

In the benchmark study, the sensitivity of the numerical model to certain parameters like mesh resolution and element type was investigated in the buckling analysis and the ultimate capacity was determined using varying analysis methods. Initial imperfections of the structure were also considered in the form of global deflection, plate initial deflection, column type initial deflection of stiffeners and sideways initial distortion of stiffeners.

1.2 Problem definition and objectives

A number of procedures on ultimate strength analysis are already established in classification rules and other recognized text. It, therefore, stands to reason that buckling results obtained from either physical tests, analytical calculations or FEA should be within reasonable agreement for any given stiffened plate structure. Without complete agreement between the FEA models, calculation methods and experiments, an acceptable level of uncertainty is required to compare the various results. This uncertainty level is provided by the aforementioned established procedures. The reference study aimed to discover the effects of class rule interpretation, numerical approaches and analysis methods on ultimate strength prediction. The results obtained from the study participants were then compared to the reference experiment to provide an understanding as to the influence of the aforementioned factors. Upon comparison with the reference experiment, the study predicted the ultimate capacity within an acceptable limit but this was not the case for the displacement at ultimate capacity, mode and location of failure.

This thesis intends to investigate the modelling parameters or combination of parameters that could have caused the variance in buckling collapse results between the

physical test and former FEAs. To achieve the main objective of this study, the following goals have been defined:

a. Analytical estimation of the critical buckling stresses for simplified panel geometries to establish a baseline to which results from FEA for the same geometry could be compared.
b. Parametric sensitivity studies of factors that affect the ultimate strength capacity of stiffened plate structures. This would be done by running non-linear FEAs of all panel geometries being considered using the FE software Abaqus.

1.3 Assumptions and limitations

In the limit state design of a given structure, a number of factors involve large degrees of uncertainty. Of these factors, only the fabrication-related initial imperfections have been considered. This includes initial distortion and residual stresses.

The participants of the study upon which this thesis is based relied on mesh sensitivity studies, knowledge and experience in the selection of optimal mesh size. These mesh sizes ranged from 12.5 x 12.5 mm to 56 x 70 mm for all sets of participants. As a result, no mesh sensitivity study has been carried out and a mesh size of 25 x 25 mm has therefore been selected and used for all models.

The material model used for all FEAs in this thesis has been limited to an elastic-perfectly plastic model.

1.4 Thesis outline

The structure of this thesis is in six chapters. The first chapter gives an introduction and provides background information on the basis of the research, assumptions made and the limitations encountered in the course of the research. The second chapter presents the relevant information obtained from literature study. The third chapter describes the methods utilized in achieving the aims stated in chapter one. Chapter four presents the results from all the analysis carried out. Chapter 5 discusses the results and compares these results to the reference study. Subsequent parts would include a conclusion, possible future work.

2 Literature study

This section provides a summary of various scientific papers published on the subject of ultimate strength. It is focused on reviewing papers that present empirical models which could be used in the evaluation of the compressive ultimate strength of stiffened plate structures. A summary of the reference study upon which this thesis is based will also be given in this section.

2.1 Empirical formulations for ultimate strength

As evidenced by Lin (1985), Paik & Thayamballi (1997) and Zhang & Khan (2009), it is possible to estimate the ultimate strength capacity of stiffened plate structures using analytical formula. These empirical formulations are based on results from non-linear FEA of a number of sample stiffened panels and fundamental theories of stiffened panel buckling like those presented by Paik & Thayamballi (2003). These formulas can be used to calculate the ultimate strength in relation to the equivalent yield strength. The formula considered has been formulated for stiffened panels subjected to axial compression. This relationship is expressed as:

$$\sigma_{xu}/\sigma_{Yeq} \tag{2.1}$$

where:

$\sigma_{xu} =$ ultimate strength of stiffened panel subjected to axial compression
$\sigma_{Yeq} =$ equivalent yield strength of the stiffened panel material

While modelling ship longitudinal strength, Lin (1985) presented an expression for calculating the ultimate strength of hull girders. Hull girders can in principle be considered as stiffened panels.

$$\sigma_{xu}/\sigma_{Yeq} = \frac{1}{\sqrt{0.960 + 0.765\lambda^2 + 0.176\beta^2 + 0.131\lambda^2\beta^2 + 1.046\lambda^4}} \tag{2.2}$$

Paik & Thayamballi (1997) present a different method of estimating ultimate strength by carrying out statistical analysis (curve fitting) on data from a mechanical collapse test database. This method resulted in the expression:

$$\sigma_{xu}/\sigma_{Yeq} = \frac{1}{\sqrt{0.995 + 0.936\lambda^2 + 0.170\beta^2 + 0.188\lambda^2\beta^2 - 0.067\lambda^4}} \leq \frac{1}{\lambda^2} \tag{2.3}$$

Upon analysis of buckling and ultimate capacity of stiffened panels, Zhang & Khan (2009) arrived at a different formula for ultimate strength calculation:

$$\sigma_{xu}/\sigma_{Yeq} = \frac{1}{\beta^{0.28}\sqrt{1.0 + \lambda^{3.2}}} \tag{2.4}$$

For this formulation,

$$\lambda \leq \sqrt{2} \tag{2.5}$$

$$\beta = 1 \; if \; \beta < 1 \tag{2.6}$$

In an attempt to improve the existing formula, Kim et al. (2017) introduced correction coefficients C_1 and C_2 and presented the formula:

$$\sigma_{xu}/\sigma_{Yeq} = \frac{1}{C_1 + e^{\lambda^2}} + \frac{1}{C_2 + e^{\sqrt{\beta}}} \tag{2.7}$$

Kim et al. (2017) proposed correction coefficients of 0.8884 and 0.4121 for C_1 and C_2, respectively. This gives the expression:

$$\sigma_{xu}/\sigma_{Yeq} = \frac{1}{0.8884 + e^{\lambda^2}} + \frac{1}{0.4121 + e^{\sqrt{\beta}}} \tag{2.8}$$

This expression holds true for column slenderness coefficient values in the range:

$$0.5 \leq \lambda < 5.0 \tag{2.9}$$

By implementing data processing techniques, Kim et al. (2019) presented a refined formula for calculating the ultimate strength of stiffened panels:

$$\frac{\sigma_{xu}}{\sigma_{Yeq}} = \begin{bmatrix} c_0 + \left(c_1 + c_2\sqrt{\lambda} + \frac{c_3}{\beta} + c_4\frac{h_w}{t_w} + c_5\sqrt{\frac{I_{pz}}{I_{sz}}}\right)\sqrt{\lambda} & + \left(c_6 + \frac{c_7}{\beta} + c_8\frac{h_w}{t_w} + c_9\sqrt{\frac{I_{pz}}{I_{sz}}}\right)\frac{1}{\beta} \\ + \left(c_{10} + c_{11}\frac{h_w}{t_w} + c_{12}\sqrt{\frac{I_{pz}}{I_{sz}}}\right)\frac{h_w}{t_w} & + \left(c_{13} + c_{14}\sqrt{\frac{I_{pz}}{I_{sz}}}\right)\sqrt{\frac{I_{pz}}{I_{sz}}} \end{bmatrix} \tag{2.10}$$

This formula although refined is only applicable to T-bar stiffened panels. Kim et al. (2019) achieved this by incorporating a polynomial function shape. This proves more accurate than the correction coefficients (C_1 and C_2) introduced by Kim et al. (2017):

$$f(x) = c_0 + c_1x + c_2x^2 + \cdots + c_{n-1}x^{n-1} + c_nx^n \tag{2.11}$$

where c_i is a real number/polynomial coefficient.

2.2 Factors affecting the ultimate capacity of stiffened plate structures

Looking at studies by Lin (1985), Paik & Thayamballi (1997) and Zhang & Khan (2009) and conversely, those by Kim et al. (2017, 2019), a trend can be observed in their prescribed formula for ultimate strength. The ultimate capacity of stiffened panels in all cases is predicated on the plate and column slenderness coefficients β and λ.

Paik & Thayamballi (2003) put together possible factors that could influence the ultimate capacity of stiffened plate structures. These factors could be:

a. Geometric
b. Material
c. Fabrication related
d. Temperature
e. Dynamic/Impact
f. Age-related degradation
g. Accident-induced damage
h. Human

Of the factors above, the geometric, material and fabrication-related factors hold significance with the empirical models presented by Kim et al. (2019).

2.3 Non-linear finite element analysis

It is possible for cracks to appear in a grillage structure when under compression or be an inherent defect in a structural member. Cracks present an extreme case of initial imperfections and distortions which is a factor that could influence ultimate capacity. Du et al. (2016) investigated the effects of such geometric imperfections on the ultimate strength of a simple stiffened panel. They tudied the influence of crack initiation, propagation/growth together with plate thickness on the ultimate strength of a sample stiffened plate. By varying the plate thickness and crack location, a comparative study of the resultant ultimate strength was possible. Non-linear FEA was done using ANSYS and a plate of dimensions 580 mm x 500 mm and crack of size 250 mm x 3mm. Upon analysis, it was found that the presence of longitudinal stiffeners greatly improves the ultimate strength of the model. The more stiffeners are present, the higher the stiffness and ultimate strength. It was concluded that the most critical crack location was the two-edge crack and that cracks on the plate have a greater influence on the ultimate strength than those on the stiffeners.

Paik et al. (2011) presented a benchmark study in which the accuracy of the ALPS/ULSAP Maestro (2014) method of determining ultimate strength of stiffened panels was investigated. The method employed was to compare the results obtained from ALPS/ULSAP to those of non-linear finite element analysis and DNV/PULS DNV (2004). The stiffened panel used for this study is shown in Figure 2.1

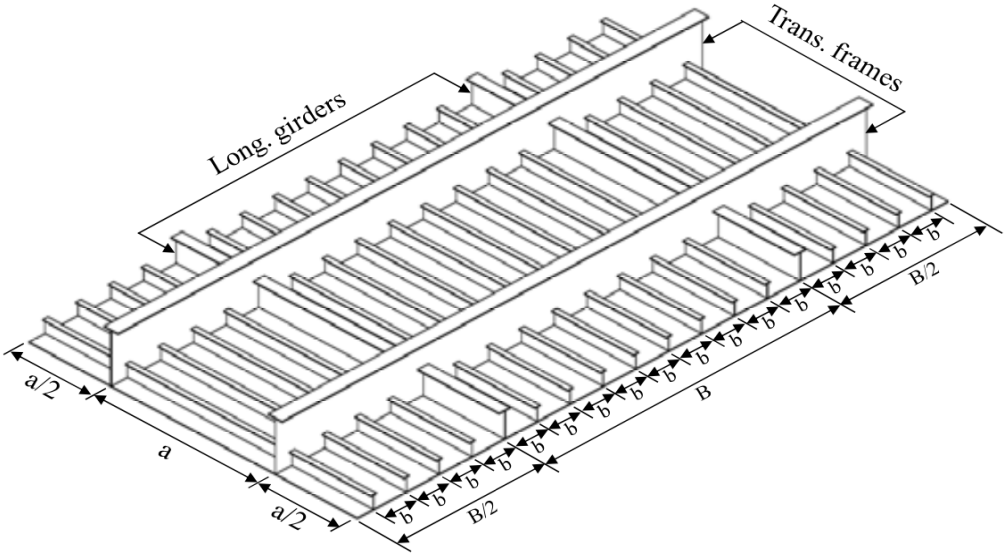

Figure 2.1: Stiffened panel used for benchmark study in Paik et al. (2011)

The study aimed to test ALPS/ULSAP prediction of ultimate strength for plates and for stiffened panels. The plate considered by Paik et al. (2011) had a length a = 2550 mm, breadth b = 850 mm and varying plate thicknesses t_p = 11, 16, 22 and 33 mm. For the material properties, yield stress σ_{yp} = 313.6 MPa, elastic modulus E = 205.8 GPa and Poisson's ratio = 0.3. The plates of varying thicknesses were then subjected to biaxial compressive loads, simply supported boundary conditions applied to all edges and initial deflection (plate buckling mode) applied. Welding residual stresses were however not considered in the study.

In this study, nonlinear finite element analysis was done using the FE software ANSYS. The amplitude of initial deflection prescribed for FEA, ALPS and ULSAP methods is given as:

$$w_{0pl} = 0.1\beta^2 t_p \tag{2.12}$$

where:

$$\beta = \frac{b}{t_p}\sqrt{\frac{\sigma_{yp}}{E}} \tag{2.13}$$

The amplitude of the initial deflection for the DNV/PULS factored in initial imperfections and was prescribed by Paik et al. (2011) as:

$$w_{0pl} = {}^{b}/_{200} \tag{2.14}$$

Paik et al. (2011) found that owning to the chosen method of implementing initial imperfection/distortion, DNV/PULS overestimates the ultimate strength of the plates. ALPS and ULSAP are however in agreement with the results obtained from FEA with ANSYS.

In the second part of the study, Paik et al. (2011) tests the validity of ALPS/ULSAP with a stiffened panel. The panel geometry is given as panel length a = 4750 mm, panel breadth B = 8550 mm, number of stiffeners = 8, plate breadth b = 950 mm and varying plate thicknesses t_p = 11, 12.5, 15, 18.5, 25, and 37 mm. The material properties plate yield stress, elastic modulus and Poisson's ratio remained the same as those of the plate in the first part of the study. The stiffeners were prescribed to have the same yield stress as the plate.

As in the analysis of the plates, no welding residual stresses were considered and the same plate initial distortion was applied. The column type and sideway initial distortion were given as:

$$w_{oc} = w_{os} = 0.0015a \tag{2.15}$$

Three types of stiffeners (flat-bar, angle bar, T-bar) were considered for analysis. Each stiffener type was also analyzed in four different sizes. The stiffener dimensions ranged from 150 x 17 mm to 550 x 35 mm for the flat-bar stiffener, and from 138 x 90 x 9/12 mm to 580 x 150 x 15/20 mm for the angle-bar and T-bar stiffeners. The stiffened panel with these stiffener dimensions were then analyzed under longitudinal compression, transverse compression, biaxial compression and combined longitudinal compression and lateral pressure loads.

Following this approach, Paik et al. (2011) were able to validate the accuracy of the ALPS/ULSAP method and found it to be in good agreement with the FEA results. They concluded that under longitudinal compression, ALPS/ULSAP underestimated the ultimate strength of large flat-bar stiffeners. Under transverse compression, ALS/ULSAP overestimates the ultimate strength for panels with thick plates and relatively weak stiffeners. This happens because the load limit of the longitudinal stiffeners is overly inflated. Under biaxial compression, no special considerations or exceptions were observed. Under combined longitudinal compression and lateral pressure loads, the loading ratio, direction of pressure application and panel dimensions all influenced the panel collapse modes.

Assessing the results of the study by Paik et al. (2011), a correlation between the column slenderness ratio and the ultimate strength of stiffened panels subjected to compression was established. This correlation exists for moderate and small stiffeners which correspond to relatively large column slenderness ratios. For stiffened panels with small values of column slenderness ratio, no correlation exists.

2.4 Reference experiment

The study by Ringsberg et al. (2021) was based on a reference experiment done in the NSWCCD's grillage test fixture, see Figure 2.2.

Figure 2.2: NSWCCD grillage test fixture (Ringsberg et al., 2021)

This fixture is capable of testing stiffened panels up to the length l = 7320 mm and width w = 2440 mm. The fixture can exert loads in the longitudinal direction (both compression and tension) of up to 22 MN. The required load is applied through 2 rows of five 2.2 MN actuators and the test structure is bolted to a heavy steel header.

The experiment was carried out on a stiffened panel structure designed by NSWCCD and fabricated by the US Army's Aberdeen test center. The stiffeners used are T-bars for both longitudinal and transverse stiffening. The panel was fabricated from A36 steel grade and had a length of 7315 mm and a width of 2438 mm. The transverse stiffener spacing was 1829 mm and the spacing for the longitudinals was 610 mm. All spacing measurements were center to center.

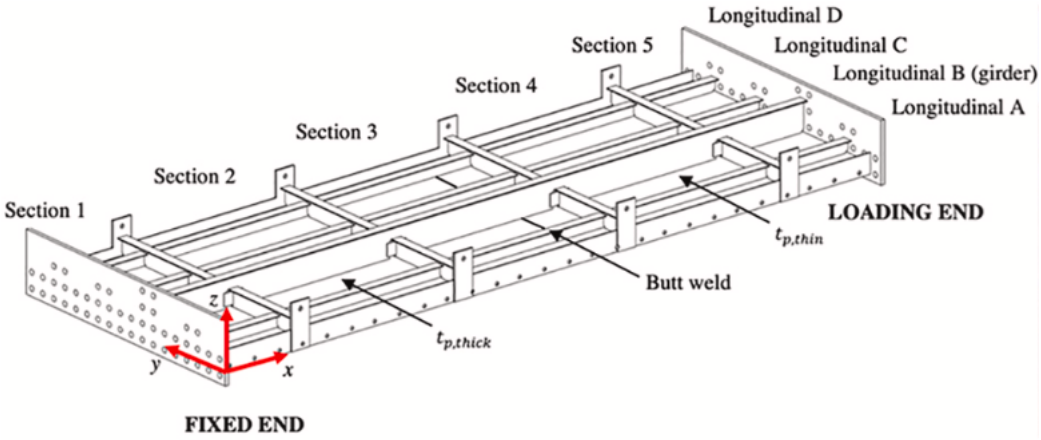

Figure 2.3: Stiffened panel used in the reference experiment presented in Ringsberg et al. (2021)

The bottom plate field of the panel was fabricated with plates of varying thicknesses 6.35 mm and 7.94 mm. The 6.35 mm plate was 3352 mm long and the 7.94 mm plate was 3962 mm long. Both were butt welded to produce the full length of 7315 mm. The panel also had side plates (9.53 mm), transverse stiffener cap plates (19.05 mm) and heavy end plates (38.10 mm). The gas metal arc welding process (GMAW-P) was used for all joinery. Details of the stiffened panel are shown in Figure 2.3. For detailed description of the experiments, see Ringsberg et al. (2021).

Figure 2.4: The stiffened panel fitted in the NSWCCD grillage test fixture; photo from Ringsberg et al. (2021)

The boundary conditions applied were fixed at the bolted end and free to displace axially at the loading end. A series of 27 tiedowns (31.8 mm threaded rods) at intervals of 254 mm and 279 mm along the length of the test structure were used to constrain vertical motions. Subsequently, the test was performed preloading the test structure to 25% and then 50% of the anticipated peak load. The 25% and 50% correspond to 1.1 and 2.2 MN, respectively. After the preloading/compression cycles, the structure was loaded well into the post buckling range and the loading was terminated when the structure dropped to 70% of the peak load. The peak load recorded during loading was 6.59 MN and the compression was halted at 4.68 MN. Figure 2.4 shows the stiffened panel being studied setup in the grillage test fixture and ready for the planned loading cycles. Figure 2.5 shows the post buckling behaviour of the stiffened panels after compression.

Figure 2.5: Buckling collapse of stiffened panel, photo from Ringsberg et al. (2021)

2.5 Reference study

This thesis is a follow-up investigation of the benchmark study presented in Ringsberg et al. (2021) on the ultimate analysis of a stiffened plate structure subjected to uniaxial compressive loads. The study was overseen by the ISSC 2022 committee III on ultimate strength.

The study assessed the challenge presented by subjecting stiffened plate structures to compressive loads. This challenge lies in the accurate prediction of ultimate strength, buckling modes and more so, post-buckling behaviour. The particular benchmark study was carried out to investigate the effects of various assumptions made by participants on the ultimate capacity and failure prediction when compared to a reference experiment. Since this thesis is a follow-up investigation, the findings of Ringsberg et al. (2021) will be discussed.

The study was done in 3 phases and in each phase, more information was made available to the participants of the benchmark study. This approach aimed to establish the effects of fabrication-related imperfections like non-uniform thickness and plate distortions. Various material models were also considered in the study. For the first phase of the study, participants were provided with the nominal dimensions of the test structure and were required to make assumptions about the geometric imperfections considered. The second phase provided new information which was used to update the model from phase one. The information provided for this phase were actual thickness measurements and geometrical imperfections, distortions and deflections obtained from laser scanning of the geometry. The third and final phase considered full stress-strain curves for all structural members obtained from tensile test results. This phase included an optional step of modelling (no measurements were provided) residual stresses and their resultant effect on the ultimate capacity and post-buckling behaviour. The third phase was therefore the most detailed as it also contained all the information added to the model from previous phases.

Using Abaqus/CAE, ADINA, ANSYS, LS-DYNA and MSC Marc models of increasing complexity were created corresponding to the aforementioned test phases. Mesh sensitivity study was also done by half of the participants and arrived at mesh sizes ranging from 12.5 x 12.5 mm to 50 x 50 mm. The rest of the participants relied

on previous knowledge and experience in the field of ultimate capacity prediction and FE analysis. These participants arrived at mesh sizes ranging from 25 x 25 mm to 56 x 70 mm. The study found the predicted ultimate capacity to be within acceptable limits for its various phases. Figure 2.6 to Figure 2.8 show the collated force-displacement curves from selected phases of the study.

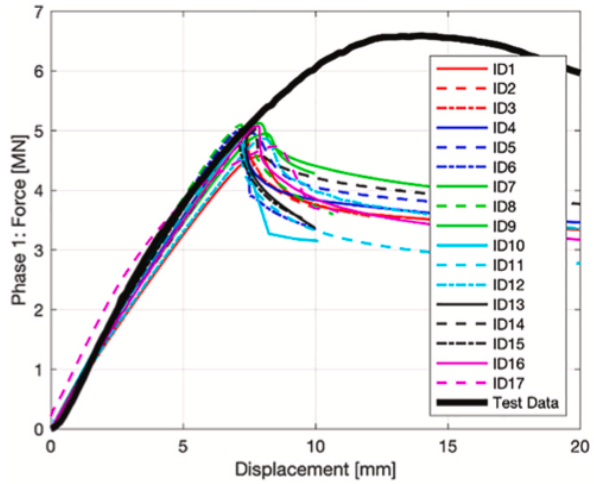

Figure 2.6: Force displacement curve from phase 1 from Ringsberg et al. (2021)

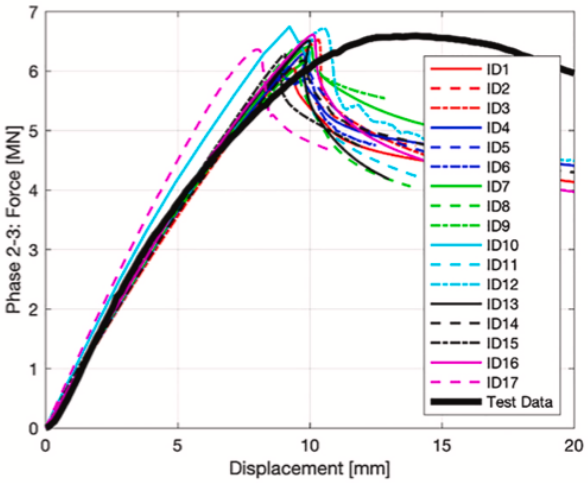

Figure 2.7: Force displacement curve from phase 2-3 from Ringsberg et al. (2021)

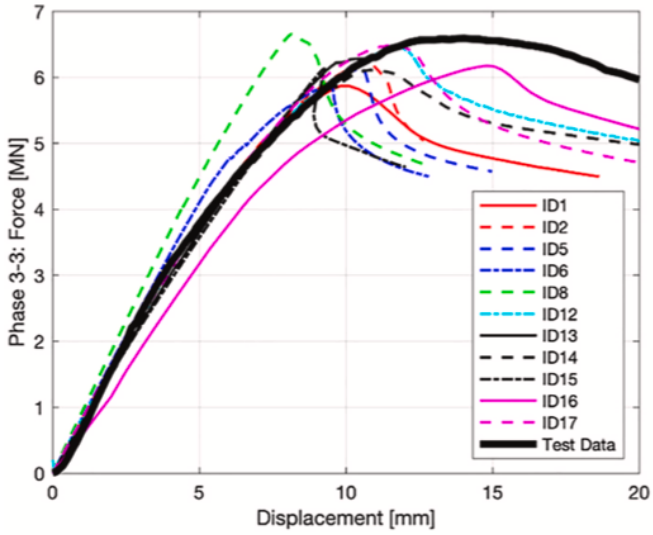

Figure 2.8: Force displacement curve from the final phase 3-3 from Ringsberg et al. (2021)

The modes and locations of failure predicted by the study participants are shown in Figure 2.9 to *Figure* 2.11.

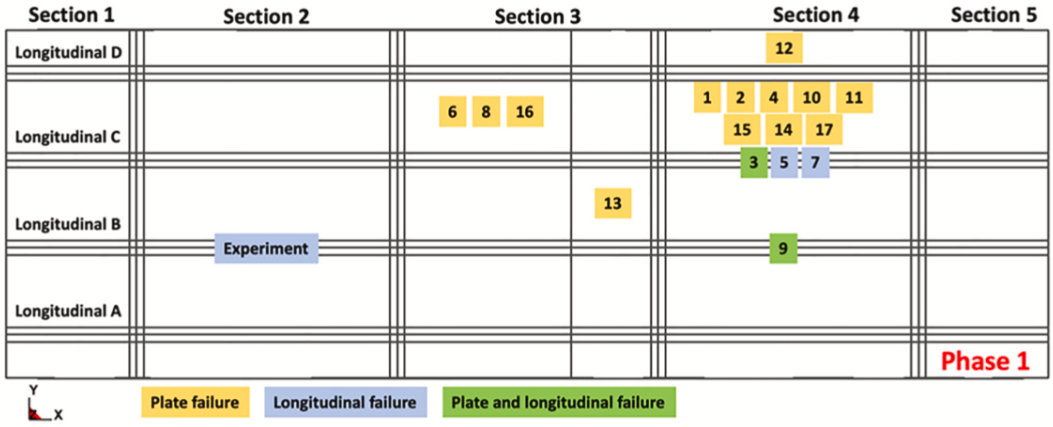

Figure 2.9: Modes and location of failure in phase 1 from Ringsberg et al. (2021)

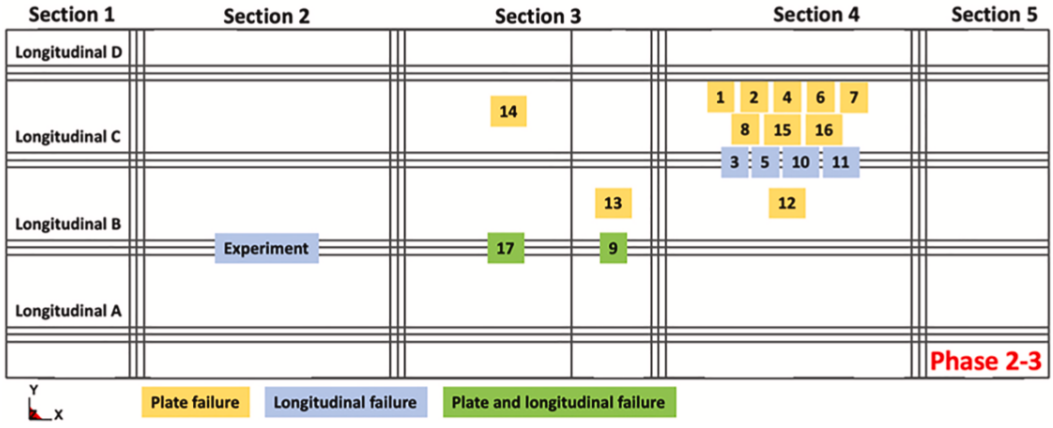

Figure 2.10: Mode and location of failure in phase 2-3 from Ringsberg et al. (2021)

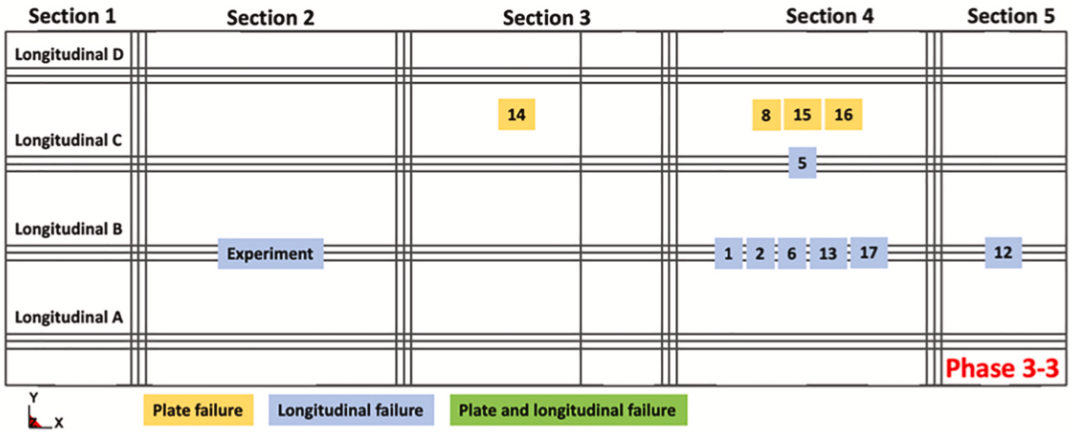

Figure 2.11: Mode and location of failure in the final phase 3-3 from Ringsberg et al. (2021)

3 Methods

This section describes the processes utilized in achieving the aim of the thesis. The analytical solution part investigates the critical buckling stresses for the geometries considered. The geometry modification delves into the changes made to the reference geometry that resulted in changes to the expected outcome. The modified panels are subjected to eigenvalue buckling analysis and the results are compared to the critical buckling stresses obtained from analytical calculations. The simulation setup applied to all geometries considered is also discussed in this section.

3.1 Estimation of ultimate capacity using empirical models

The ultimate capacity for a simplified geometry similar to the reference geometry has been calculated to obtain a baseline from which to investigate other geometries. It may also be of interest to estimate the variance in the ultimate capacity due to initial imperfections.

Using equation (2.10) in chapter 2.1, the ultimate capacity of sample stiffened plate structures have been calculated. The sensitivity of the ultimate capacity to plate and column slenderness ratios have been investigated by varying the thickness of the bottom plate field and stiffener size used in the calculations. The models used for analytical calculations designated panels A and B are derived from the model in the study by Ringsberg et al. (2021), and as such, the material properties are kept consistent with the study. Panels A and B correspond to LS2, LS3, LG2 and LG3 for plate thicknesses 6.35 and 7.94 mm as shown in Table 3.2. These panels are part of a number of models subjected to non-linear FEA. Table 3.1 shows the geometric properties of the panels. The plate thicknesses used for calculation are 6.35, 7.94, 12.35, 17.94, and 22.35 mm. Plate thicknesses 6.35 mm and 7.94 mm correspond to the plate thicknesses used for non-linear FEA. Additional plate thicknesses of 12.35, 17.94, and 22.35 mm have also been studied. This gives an in-depth understanding of the bottom plate field and how a wide range of plate thicknesses would influence its behaviour in compression.

An assessment of the influence of the bottom plate thickness, stiffener size and configuration on these simplified geometry would provide a closed form estimate of the ultimate capacity. This ultimate capacity estimate can then be studied along with the estimates from FEA for similar models to better understand how they compare. For simplicity, only models with uniform plate thickness and longitudinal stiffeners have been considered.

3.2 Software requirement

3.2.1 Python

The open-source software Python version 3.9.5 has been used to implement the selected empirical model. A script from which normalized values of the compressive ultimate strength will be calculated has been developed. Spyder IDE version 5.3.2 was used to run python.

3.2.2 Simulia Abaqus/CAE

The commercial software Abaqus/CAE 2022 Dassault Systèmes Simulia Corp. (2022) has been used for all analyses. Abaqus is a FE software and its complete Abaqus environment (CAE) provides a platform for FE modelling, simulation and subsequent visualization of results. Abaqus provides a number of FE solvers but for the purpose of

this thesis, the general static solver will be used to resolve a number of quasi-static cases. A description of the simulation steps for each model analyzed is given below. A static general analysis step is added in the abaqus step module. The time period is set to 1 and the maximum number of increments to 100000. The initial and maximum increment size are set at 0.0005 and 0.005 respectively. Field and history output requests are created in this module. Interaction and load modules are set and a mesh (25 x 25) mm is applied to the model. A full analysis is then created and run for each model and the results displayed in the the visualization window. All steps of the analysis are executed in the Abaqus CAE graphic user interface (GUI). The reaction forces and displacement data are saved from abaqus as text files and used to plot load – displacement curves shown in subsequent sections.

3.3 Modelling

The nominal model used by Ringsberg et al. (2021) in phase one of the reference study is used as the reference geometry prescribed as BM1. Keeping the material consistent with the reference study, ASTM A36 steel properties are applied to the model. General and mechanical material behaviour are prescribed as density (ρ), young's modulus (E) and poisson's ratio (ν) respectively. Density of steel is applied as (7850 kg/m3). The elasticity properties for young's modulus and poisson's ratio are set at (200000 MPa and 0.26). An elastic – plastic (EP) material model is used for all models studied.

3.3.1 Reference geometry

The model obtained from the reference study forms the basis of the thesis and model modifications. The model is consistent with the stiffened panel built for the reference experiment and used in the benchmark study by Ringsberg et al. (2021). The structural members have been colour coded as seen in Figure 3.1. Two colours (cream and green) have been assigned to the bottom plate field to represent the different plate thicknesses. The green portion corresponds to a plate thickness of 7.94 mm and the other to 6.95 mm plate thickness. Different colours have also been applied to the longitudinal stiffeners, girder, side plates, transverse frame caps and other structural members for easy identification. The dimensions of the longitudinal stiffeners correspond to AISC W12 X 14 beams, the lone girder corresponds to AISC W12 X 19 beams and the transverse stiffeners to AISC W10 X 17 beams.

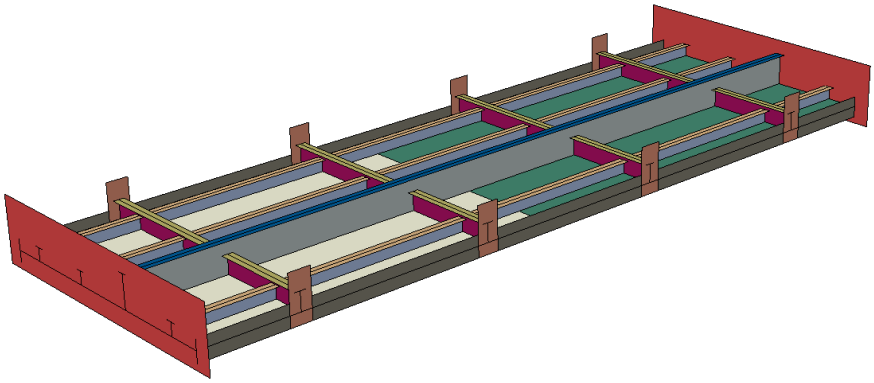

Figure 3.1: Base model geometry (BM1)

The dimensions of the plates, stiffeners and girders have been detailed in Table 3.1 below.

Table 3.1: Geometry definition

Definition	Description	Value	Unit
Plate			
t_1	Thick plate thickness	7.94	mm
t_2	Thin plate thickness	6.35	mm
Longitudinal stiffener			
H	Web height	124.62	mm
b_f	Flange width	100.84	mm
t_f	Flange thickness	5.72	mm
t_w	Web thickness	5.08	mm
A		1206.45	mm^2
Longitudinal girder			
h	Web height	308.86	mm
b_f	Flange width	101.73	mm
t_f	Flange thickness	8.89	mm
t_w	Web thickness	5.97	mm
A		2718.7	mm^2

3.3.2 Geometry modification

To study the post-buckling behavior of the stiffened panel, modifications were made to the reference model to investigate the parameters or combination of parameters that significantly influenced the results from the benchmark study. To achieve this, the relationship between the bottom plate field thickness, the choice of stiffener and the stiffener configuration was studied. The modifications made to come up with these geometries have been somewhat simplified to make the analysis as simple as possible and as such, the geometry of the transverse stiffeners has remained unchanged and is therefore the same across all models studied. Upon modification of the base model, the geometry to be considered for analysis has been created and presented in the figures below.

To study the influence of the plate characteristics on the ultimate capacity of the stiffened panel, one of the modifications made was creating a bottom plate field with uniform thickness and observing how this alters the results obtained from analysis of a similar model in which the bottom plate field is a combination of different plate thickness as in Figure 3.1. Cases wherein the bottom plate has been modified are shown in Figure 3.2 and Figure 3.3.

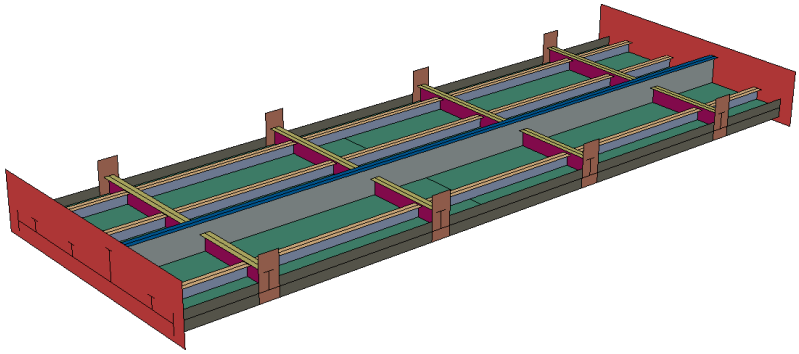

Figure 3.2: Base model with uniform bottom plate field (7.94 mm) (BM2)

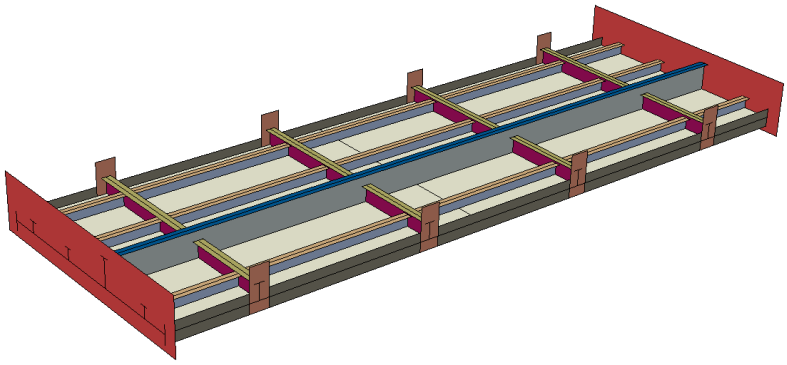

Figure 3.3: Base model with uniform bottom plate field (6.35 mm) (BM5)

A model case where there is no longitudinal girder present is shown in Figure 3.4. The dimensions of the longitudinal girder have been applied to all stiffeners which gives us a case with a varying bottom plate field and significantly larger longitudinal stiffeners.

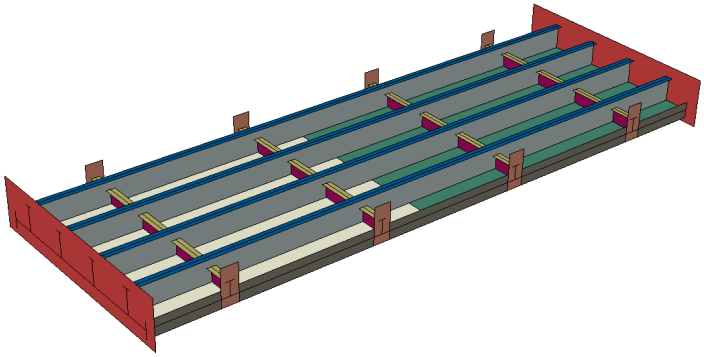

Figure 3.4: Varying bottom plate field with longitudinal girders (LG1)

Similar to Figure 3.4, the model in Figure 3.5 has a varying bottom plate field and uniform longitudinal stiffeners with much smaller dimensions.

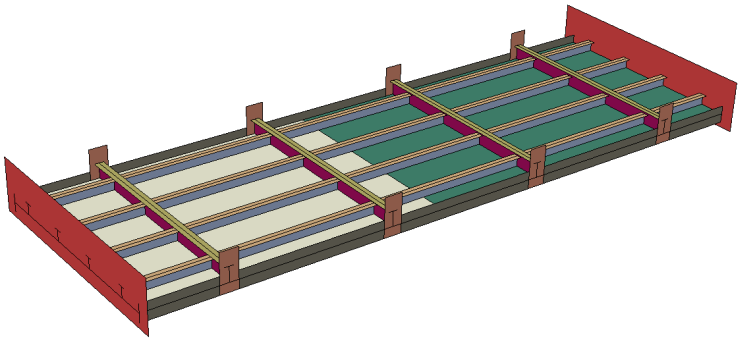

Figure 3.5: Varying bottom plate field with longitudinal stiffeners (LS1)

The dimensions to be considered when either longitudinal girder or stiffener is mentioned are those presented in Table 3.1.

Table 3.2: Model description

Model	**Details**
BM1	The base model used in the reference study.
BM2	Same as BM1 but with a uniform plate field
BM3	The same setup as the base model except the direction of applied force.
BM4	Base model with displacement and rotation free for all axis
BM5	Same as BM2 but with a different bottom plate thickness
LG1	Model alteration wherein all the longitudinal stiffeners are the same dimensions as the longitudinal girders on the base model.
LG2	Same as LG1 but with a uniform plate field
LG3	Same as LG2 but with a different bottom plate thickness
LS1	Model alteration wherein the longitudinal girder has the same dimensions as the longitudinal stiffeners on the base model.
LS2	Same as LS1 but with a uniform plate field
LS3	Same as LS2 but with a different bottom plate thickness

The method of naming the models is a function of the longitudinal stiffener configuration. The base model and all its derivatives are prescribed (BMx) where "x" depends on the bottom plate field, force direction, force location and applied boundary conditions. All cases where the dimensions of the longitudinal girder are applied to all longitudinal stiffeners are prescribed (LGx). For cases where the dimensions of the longitudinal girder have been reduced to correspond to the stiffeners, (LSx) is prescribed. The naming convention is presented in Table 3.2.

The combination of alterations made to the reference model results in a number of possible models. In addition to the bottom plate field and selected stiffener configuration, consideration is also given to the direction of force application, location of force application and prescribed boundary conditions. These models obtained from a combination of the aforementioned alterations and variations are tracked in a simulation matrix. An excerpt from the simulation matrix is presented in Table 3.3. It is an excerpt from the exhaustive simulation matrix included in Appendix 8.1.

Table 3.3: Model data

S/N	Task ID	Geometry	Plate thickness	Force location	Force direction	Boundary condition
1	BM1	stiffener and girder	$t_{1,2}$	EPn	(-x)	clamped
2	BM2	stiffener and girder	t_1	Epn	(-x)	clamped
3	BM3	stiffener and girder	$t_{1,2}$	EPs	x	clamped
4	BM4	stiffener and girder	$t_{1,2}$	EPn	(-x)	free
5	BM5	stiffener and girder	t_2	EPn	(-x)	clamped
6	LG1	longitudinal girder	$t_{1,2}$	EPn	(-x)	clamped
7	LG2	longitudinal girder	t_1	EPn	(-x)	clamped
8	LG3	longitudinal girder	t_2	EPn	(-x)	clamped
9	LS1	longitudinal stiffener	$t_{1,2}$	EPn	(-x)	clamped
10	LS2	longitudinal stiffener	t_1	EPn	(-x)	clamped
11	LS3	longitudinal stiffener	t_2	EPn	(-x)	clamped

The task ID (BM1, BM2,…) refers to the naming convention in Table 3.2 chosen for the models. The geometry presents the longitudinal structural members present in a given model. The plate thickness shows models with varying ($t_{1,2}$) or uniform (t_1, t_2) bottom plate fields. The location of force application is either the end plate north (EPn) or the end plate south (Eps). The direction of force application is prescribed *-x* when applied at EPn and *x* when applied at EPs. For the boundary condition, clamped describes a condition where all degrees of displacement and rotation are constrained except the axial displacement in the longitudinal direction. For the case with a free boundary condition, there is no constraint on displacement and rotation. The material model and mesh size are left unchanged as elastic perfectly plastic and 25 mm, respectively.

Referring to Chapter 2.5, the participants of the study in Ringsberg et al. (2021) presented discrepancies in the failure mode and location when compared to the reference experiment. By modifying components of the base model (BM1) used in the study and subjecting the modified models to non-linear finite element analysis, the parameters or combination of parameters influencing the failure of the structure will be investigated. The geometry modification will also provide additional insight regarding the influence of modelling practices employed on the FEA results. Force displacement curves of all models studied will also be presented. This would show the effects of the modifications made on the ultimate capacity of the structure.

4 Results

In this chapter, solutions to the analytical calculation of ultimate capacity obtained by implementing empirical formulas in Python and results from non-linear FEA of modified geometry are presented.

The results obtained from the modified models have been compared to the base model. This comparison is done to better understand the influence of bottom plate field thickness, stiffener choice and configuration on the FEA results for ultimate capacity, failure modes and location. These comparisons have been categorized into a number of cases wherein the effects of the aforementioned factors are discussed. A total of 6 cases were deemed to give a satisfactory overview and are therefore presented. The eigenvalue buckling analysis, ultimate capacity, failure modes and location for each case will also be discussed.

4.1 Empirical solution for ultimate capacity

Implementing equation (2.10) in Python, the code in Appendix 8.2 was developed and used to calculate the ultimate capacity of simplified panel geometries.

Table 4.1: Results from empirical models implemented in Python

Parameter	**Value**					**Unit**
Panel A (stiffener)						
t_p	6.35	7.94	12.35	17.94	22.35	mm
σ_{xu}/σ_{Yeq}	0.4492	0.4346	0.3959	0.3499	0.3144	
σ_{xu}	112.3	108.65	98.98	87.48	78.6	MPa
P_{cr}	2.72	2.63	3.46	4.25	4.67	MN
λ	0.8247	0.8825	1.0113	1.1235	1.1803	
β	3.3963	2.7162	1.7462	1.2022	0.9649	
Panel B (girder)						
t_p	6.35	7.94	12.35	17.94	22.35	mm
σ_{xu}/σ_{Yeq}	0.6080	0.6542	0.7614	0.8547	0.8961	
σ_{xu}	152	163.55	190.35	213.68	224.03	MPa
P_{cr}	4.62	4.97	7.83	11.7	14.68	MN
λ	0.2923	0.3083	0.3474	0.3888	0.4164	
β	3.3963	2.7162	1.7462	1.2022	0.9649	

With the normalized values in Table 4.1, the compressive strength (σ_{xu}) has been calculated using the equivalent yield stress (σ_{Yeq}). The compressive strength is subsequently translated to peak load (P_{cr}) using the formula;

$$\sigma_{xu} = \frac{P_{cr}}{A} \tag{4.1}$$

$$P_{cr} = \sigma_{xu} \times A \tag{4.2}$$

where;
A is the cross sectional area of the stiffened panel. The peak loads obtained are therefore the ultimate capacity of the respective panels.

The ultimate capacity estimated using empirical models can therefore be compared to the peak load obtained from non-linear FEA for some of the models considered.

4.2 Eigenvalue analysis

The results obtained from eigenvalue based buckling analysis will be presented from Figure 4.1 and subsequently discussed. These results show the shape of the structure being considered for any given buckling mode. Figure 4.1 to
show the shape for the first buckling mode in models BM1, BM2, LG1 and LG2.

The eigenvalue analysis follows a similar pattern based on the bottom plate fields of the models shown. Models with varying bottom plate field present similar shapes for mode 1 buckling. The same applies to models with uniform bottom plate fields.

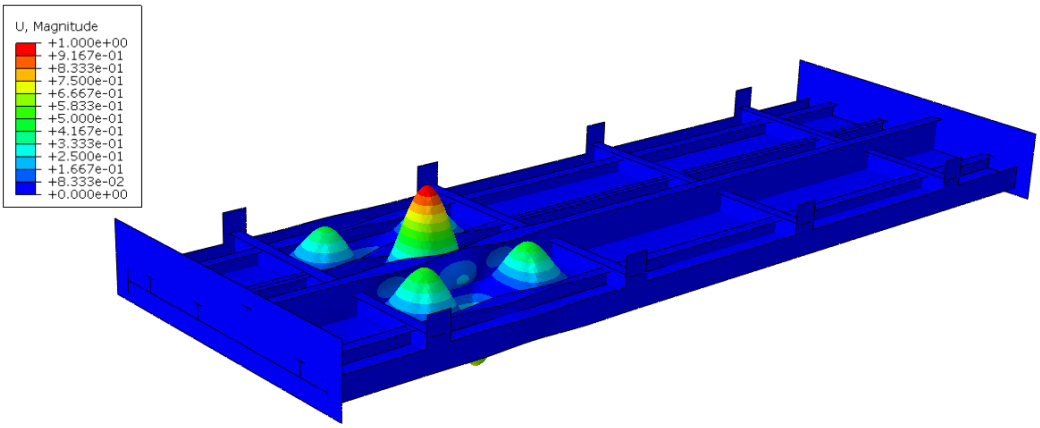

Figure 4.1: Linear buckling results for BM1 (base model)

From Figure 4.1, it appears that the linear perturbation employed for the buckling analysis correctly predicts the failure mode recorded in the reference experiment. This could be as a result of the constraint applied to the loading end of the stiffened panel in the analysis setup. Multipoint constraint (MPC) was used at thye loading end for the linear buckling analysis. This failure prediction could also be influenced by the bottom plate thickness. Since the model in Figure 4.1has a varying bottom plate field, it is possible that an average plate thickness was used during the analysis. The plate thickness theory could be corroborated by the FEA results for models with thin plate bottom plate field.

An asymmetry of the buckling shape with respect to the mid section observed in the model Figure 4.2 could be attributed to force imbalance caused by applied boundary conditions. This asymmetry could be caused by modelling error or quite possibly still be influenced by plate thickness.

The buckling shape for models in Figure 4.3 and Figure 4.4 is consistent with models having varying bottom plate fields.

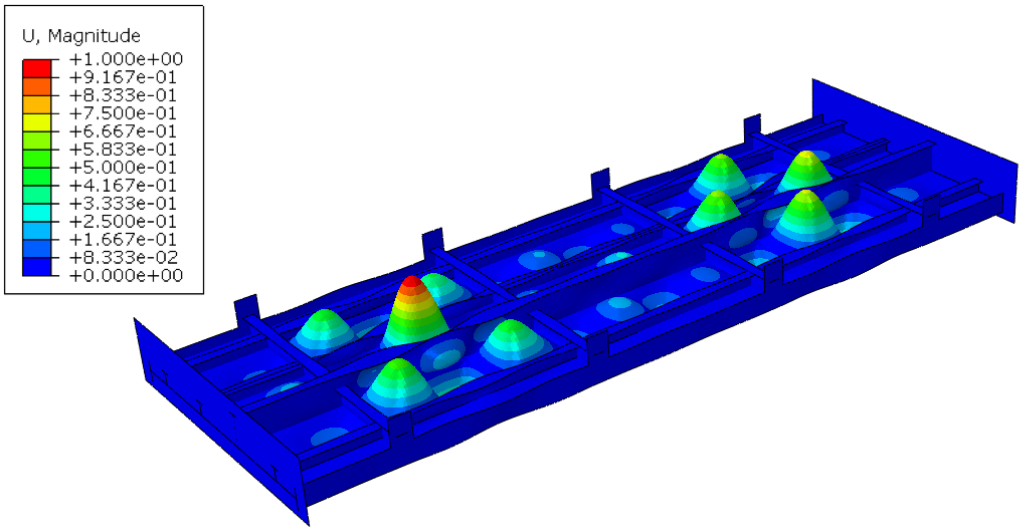

Figure 4.2: Linear buckling results for BM2 (base model with uniform plate field)

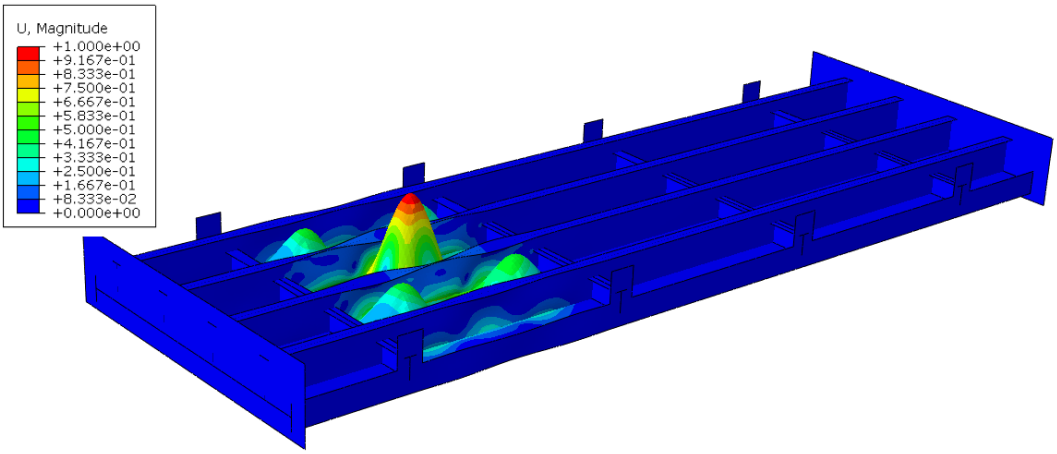

Figure 4.3: Linear buckling resuts for LG1 (girders with varying plate field)

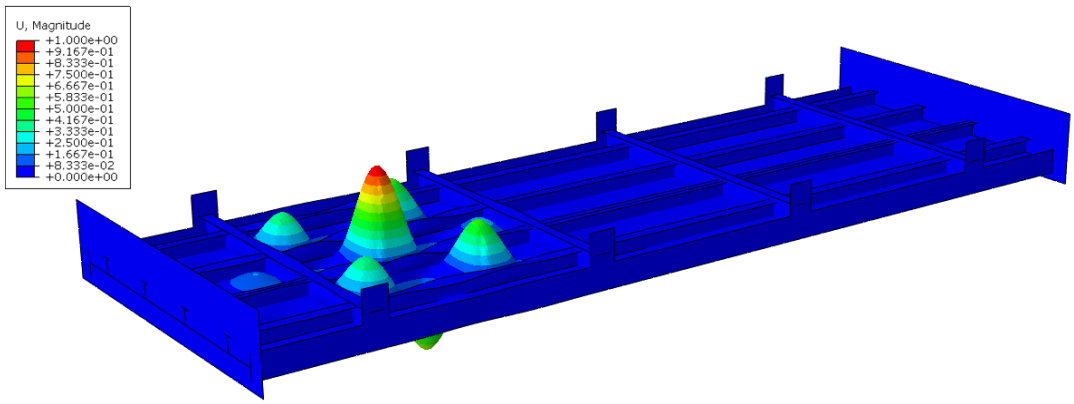

Figure 4.4: Linear buckling results for LS1 (stiffeners with varying plate field)

4.3 FE prediction of ultimate capacity

Case 1

For this case, the base model (BM1) has been compared to models BM2 (uniform bottom plate field of 7.94 mm), BM3 (different direction of force application, *x*), BM4 (free displacement and rotation) and BM5 (uniform bottom plate field of 6.35 mm). The ultimate capacity of the later models follows the trend established by BM1.

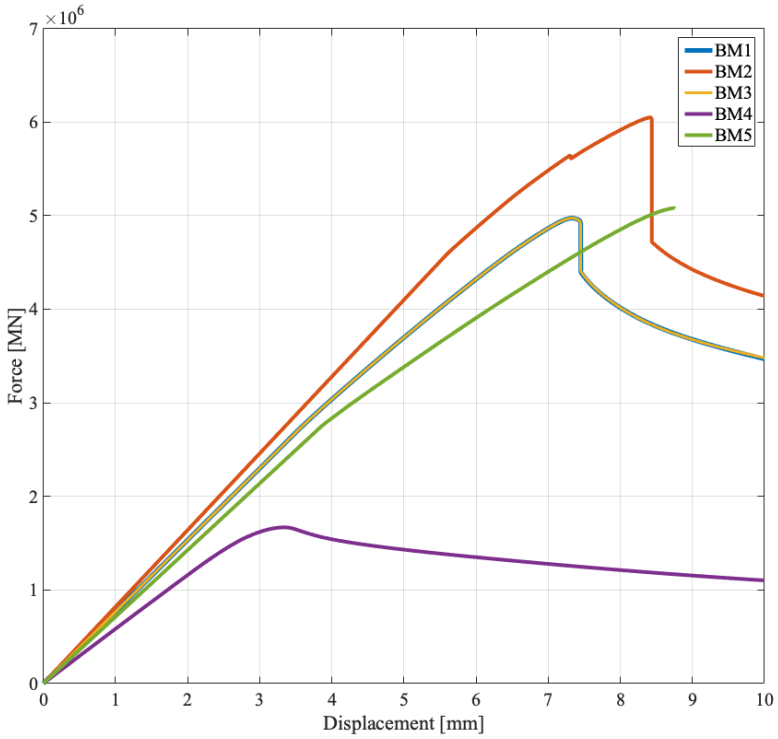

Figure 4.5: Force displacement curve comparing all BMx models

In this case, the stiffener configuration is exactly the same. The differences between BM1 and the other 3 models considered are the bottom plate field in the case of (BM2), the direction of force application (BM3) and the applied boundary conditions (BM4) and the effect of these changes on the ultimate capacity of a sample model. BM2 has the highest ultimate capacity 6.05 MN as expected for a uniform bottom plate field. BM4 has a comparatively low ultimate capacity of 1.67 MN which is to be expected for a model with no translational and rotational constraints. It is interesting however to note that BM3 has the exact same ultimate capacity and post-buckling behaviour as the base model (BM1). This implies that the force application criterion has little to no effect on the ultimate capacity. BM5 has an ultimate capacity consistent with uniform plate fields but fails to show the post buckling behaviour of the model. This may be as a result of the displacement control applied while setting up the model.

Case 2

For this case, the ultimate capacity results for the models LS1 and LS2 where the longitudinal girder has been replaced by a regular stiffener are compared. It also confirms the trend observed in case 1 for uniform and varying plate fields. The observed trend in case 1 is validated here. The model with a uniform bottom plate (7.94 mm) field (LS2) in this case results in a higher ultimate capacity when compared to one with varying plate fields (LS1).

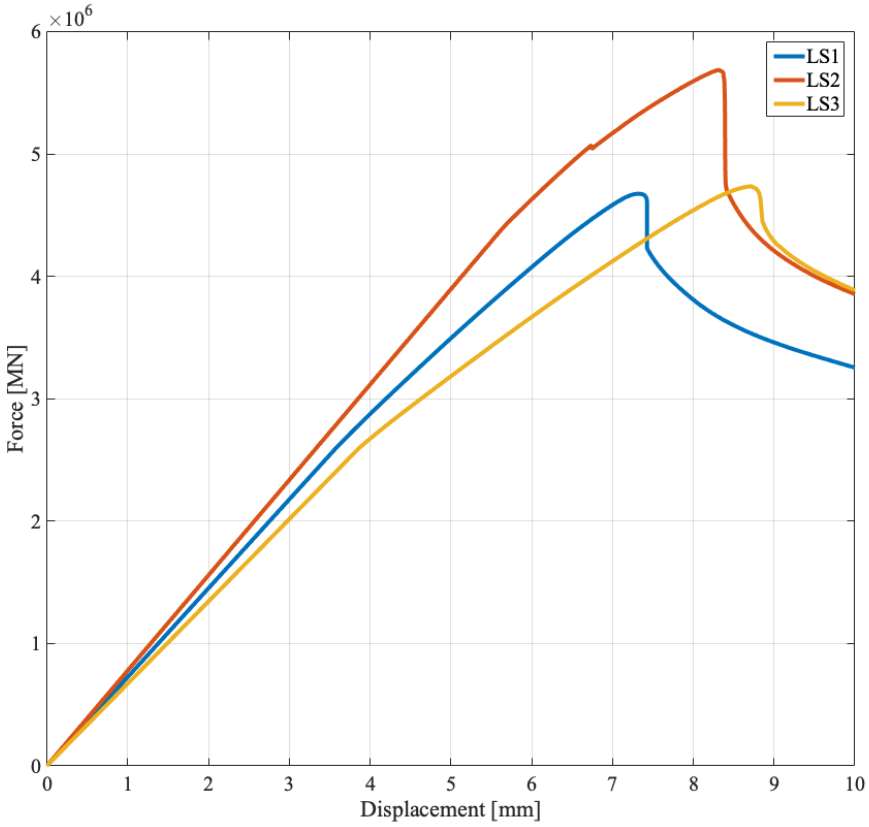

Figure 4.6: Force displacement curve comparing LS1 (varying plate field), LS2 (uniform plate field thickness 7.94 mm) and LS3 (uniform plate field thickness 6.35 mm)

LS2 shows a much higher ultimate capacity than other LS model as shown in Figure 4.6 This is an evident indication of the additional load a uniform plate field is able to withstand. Local longitudinal flange and web failure occur at load and displacement of 5 MN and 6.5 mm, respectively. The model is however able to withstand an additional load of 0.67 MN before a peak capacity of 5.67 MN is attained.

Case 3

Similar to case 2, ultimate capacity results for the models LG1 and LG2 where the dimensions of the longitudinal girder have been applied to the longitudinal stiffeners. The longitudinal stiffeners are therefore larger than previous cases and as a result have much higher ultimate capacities. The established trend of ultimate capacity level of the uniform plate field being higher than the recorded value for the varying plate field also applies here.

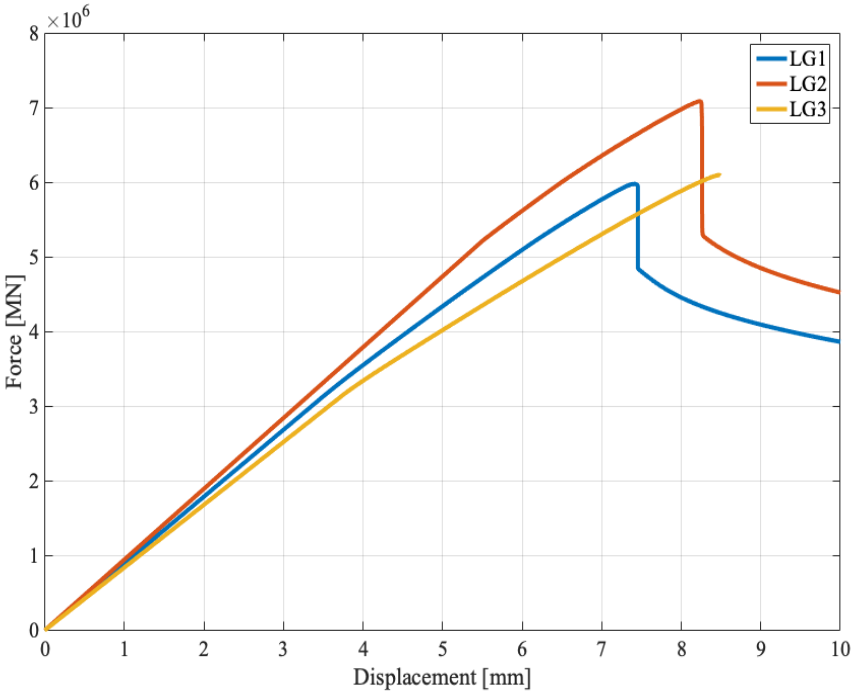

Figure 4.7: Force displacement curve comparing LG1 (varying plate field), LG2 (uniform plate field thickness 7.94 mm) and LG3 (uniform plate field thickness 6.35 mm)

In this case, however, although the ultimate capacity is much higher than in previous cases, there is an abrupt and significant drop after its peak capacity. This drop may be interpreted as the combined effect of the uniform bottom plate field and large longitudinal stiffeners. To understand this abrupt drop from the peak capacity of LG2, the method of panel collapse must be investigated. Looking at how the panel collapsed, plate failure is observed at a displacement of 7.2 mm but the panel withstood load until a displacement of 8.1 mm. This additional load is therefore attributed to the stiffener dimensions. The effects of the bottom plate field coupled with the column slenderness ratio results in a much higher peak capacity. The drop from peak capacity is therefore a result of severely diminished post-buckling strength due to stiffener failure. The higher ultimate capacity is expected from the size of longitudinal stiffeners used for LG1 and LG2. LG3 also fails to present the post-buckling behaviour and as such, the highest load attained is prescribed as the peak load. This could also be attributed to displacement control as in the case of BM5.

Cases 1-3 have compared models with a similar configuration of longitudinal stiffeners. This has shown the effects of the bottom plate field and boundary conditions on the resultant ultimate capacity. Cases 4, 5 and 6 would provide comparisons for models with similar bottom plate fields but with varying longitudinal stiffener configurations.

Case 4

For this case, ultimate capacity results for models LS1 and LG1 which have varying bottom plate fields are compared to the results from the base model BM1.

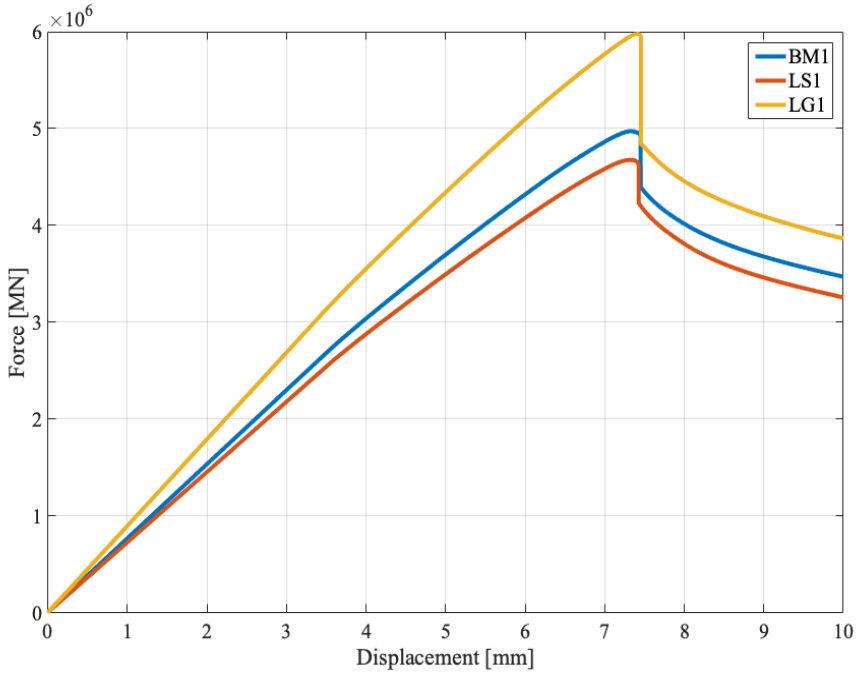

Figure 4.8: Force displacement curve comparing BM1 (base model), LS1 (stiffener with varying plate field) and LG1 (girder with varying plate field)

Case 4 shows similar displacement at ultimate capacity for both models BM1 and LG1. LG1 with much larger longitudinal stiffeners does not provide a reduced displacement than BM1 at its ultimate capacity. Although LG1 has a higher column slenderness ratio compared to BM1, it still remains unable to resist any more displacement before peak capacity is reached. This is attributed to cumulative stiffener failure in LG1 immediately after peak capacity is attained. LS1 with the smallest stiffener dimensions and no gider to compensate for this presents the lowest peak capacity.

Case 5

For this case, ultimate capacity results for models LS2 and LG2 which have a uniform bottom plate field of 7.94 mm are compared to the results from the BM2 model.

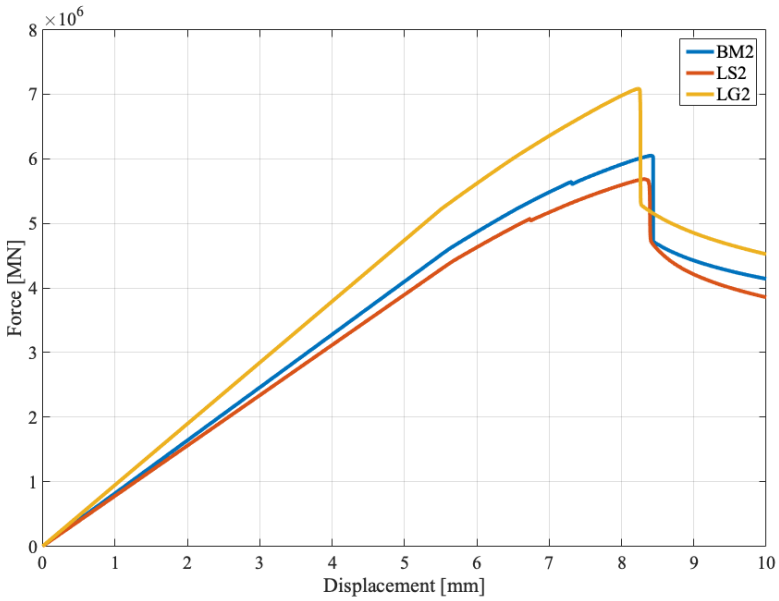

Figure 4.9: Force displacement curve comparing models BM2, LS2 and LG2 with uniform plate field 7.94 mm

Upon applying a uniform plate field on case 5, LG2 withstands even less displacement at ultimate capacity than BM2. This is attributed to the combined stiffener and plate failure in LG2 by the time peak capacity is attained. LS2 has the lowest peak capacity as expected for the stiffener dimensions used.

Case 6

For this case, ultimate capacity results for models LS3 and LG3 which have a uniform bottom plate field of 6.35 mm are compared to the results from the BM5 model.

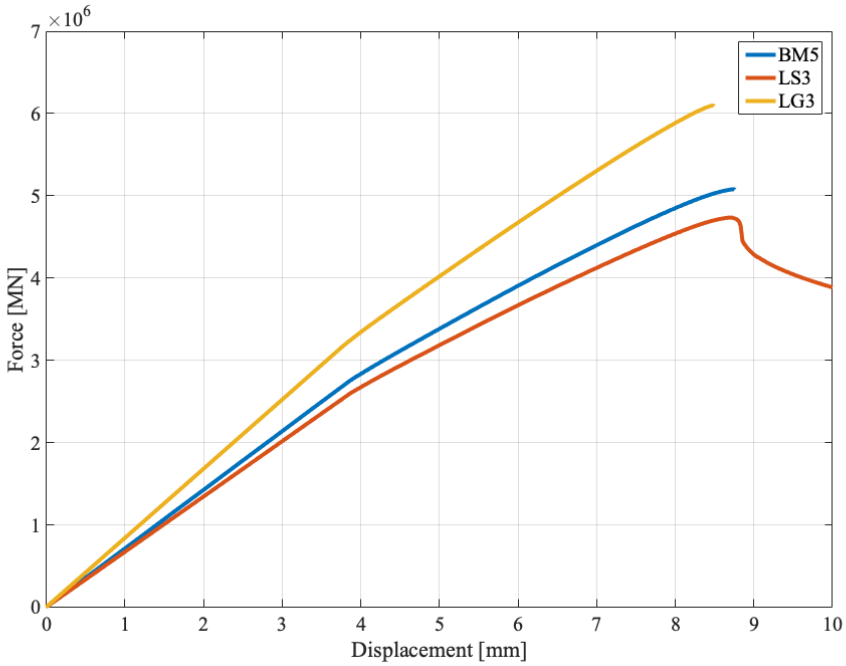

Figure 4.10: Force displacement curve comparing models BM5, LS3 and LG3 with uniform plate field of 6.35 mm

Upon applying a uniform plate field on case 6, LG3 withstands slightly less displacement at ultimate capacity than BM5. This is attributed to the reduced thickness of the bottom plate field. LS3 has the lowest peak capacity as expected for the stiffener dimensions used.

Table 4.2 shows the ultimate capacity gotten from the reference experiment, phase 1 of the reference study and all the models studied as obtained from all FEAs. It also shows the ultimate capacity estimated for some models from implementing empirical models for ultimate capacity prediction.

Table 4.2: Ultimate capacity for all studied models

Model	**Ultimate capacity FEA (MN)**	**Ultimate capacity empirical (MN)**
Reference Experiment	6.59	-
Phase 1	4.93	-
BM1	4.97	-
BM2	6.05	-
BM3	4.97	-
BM4	1.67	-
BM5	5.08	-
LG1	5.97	-
LG2	7.08	4.97
LG3	6.09	4.62
LS1	4.67	-
LS2	5.67	2.63
LS3	4.74	2.72

Looking at empirical results in Table 4.2 and comparing them to their corresponding FEA results, a lower ultimate capacity value is observed. This implies that the empirical methods used in predicting the ultimate capacity are comparatively conservative and may have some error in the assumstions made for boundary conditions and material properties. The FE model may therefore be more accurate as regards boundary conditions, material properties and geometry complexity. This ensures the contribution of the structural members to the ultimate capacity is reflected in the FEA results. This accounts for much higher ultimate capacity values.

The results from FEA are presented in Figure 4.11 as compared to the ultimate capacity recorded in the reference experiment. The results are also shown in Figure 4.12 with reference to the mean ultimate capacity recorded in phase one of the reference study. Phase one is referenced here because it is the reference model used for this thesis.

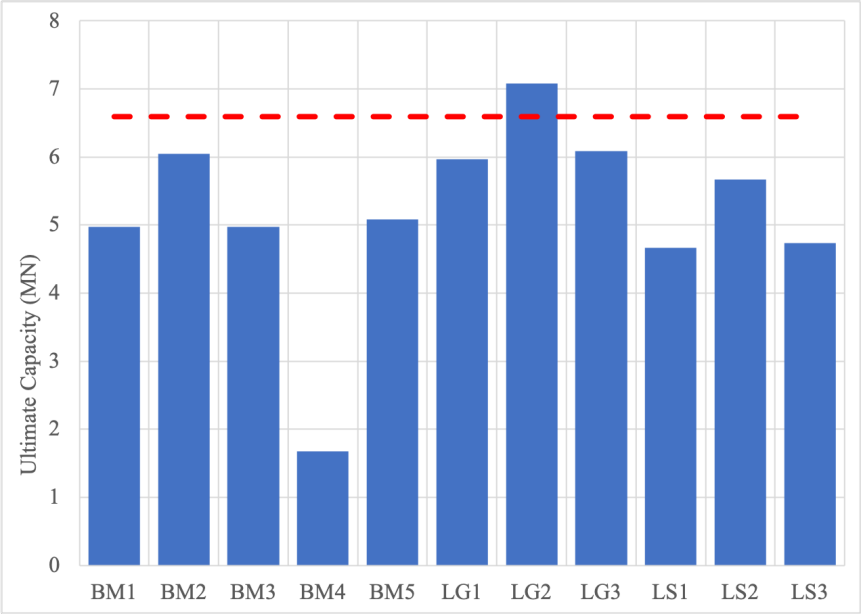

Figure 4.11: Bar plot of ultimate capacity with respect to reference experiment

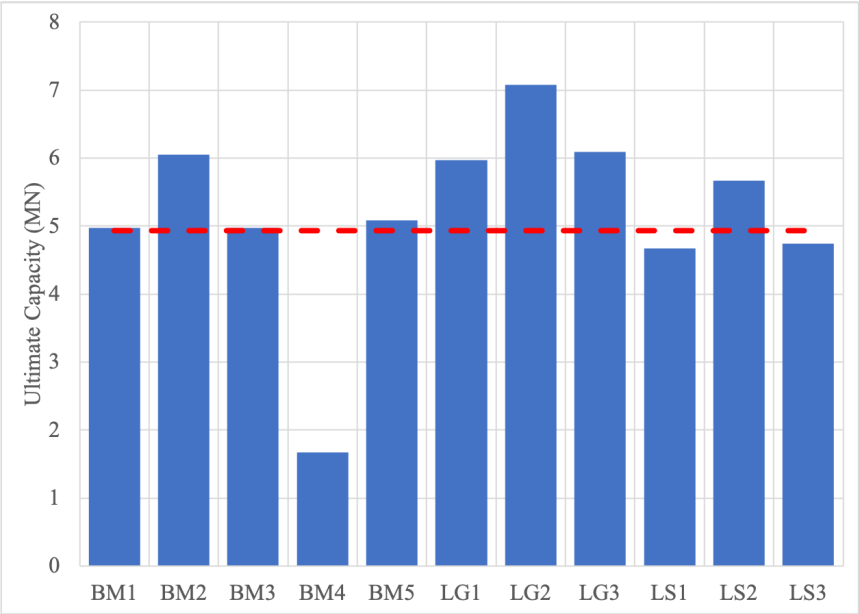

Figure 4.12: Bar plot of ultimate capacity with respect to phase 1 mean ultimate capacity

4.4 Prediction of failure modes and location

Unlike the ultimate capacity which had a direct correlation to the geometry modifications, this has not been the case for the location of failure. A similar failure mode has been recorded for most of the models studied. However, displacement control of 10mm in (-x) direction proved insufficient to capture the post buckling behaviour of the model with a uniform bottom plate thickness of 6.35mm. This prescribed displace ment was able to capture the response of the panel up to ultimate capacity. The stress state of the panel in compression at ultimate capacity is shown in Figure 4.13.

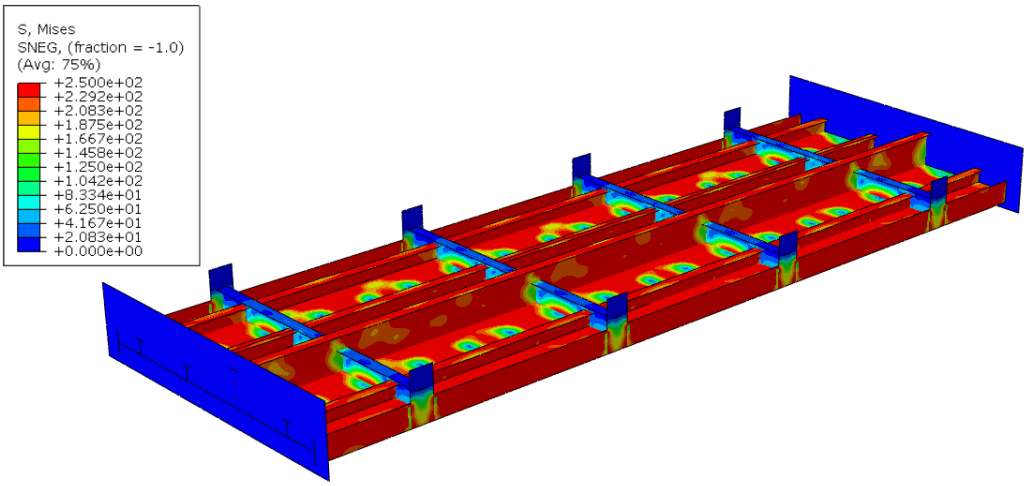

Figure 4.13: BM5 stress state at ultimate capacity

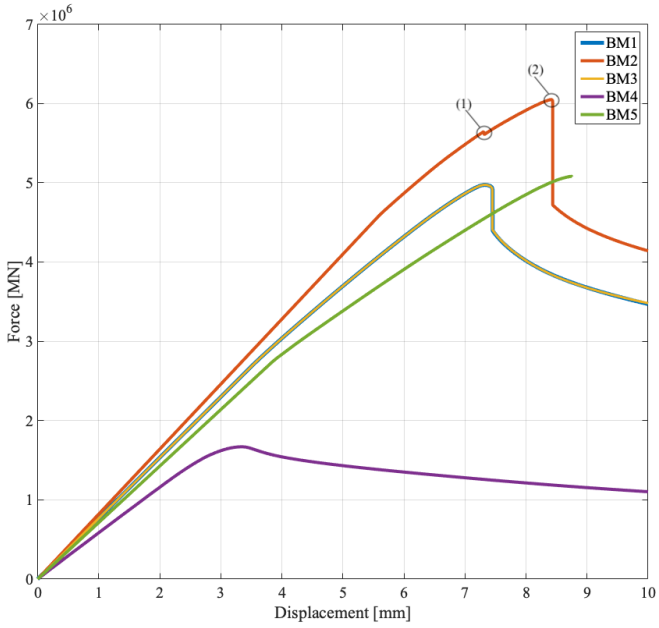

Figure 4.14: Sequence of failure recorded in BM2 and BM4 models.

The model designated BM4 in Figure 4.15 has the same geometry as BM1. It however differs from BM1 in the boundary conditions applied while setting up the analysis. The purpose of this model was to investigate the effects of rotational and translational constraints on the ultimate capacity, failure mode and location. This model was setup free to translate and rotate along and about (x, y, z) axes. Its resultant ultimate capacity and sequence of failure is shown in Figure 4.14. Compared to all other models considered where translation is only allowed in the (-x) direction, the ultimate capacity of BM4 is much lower than that of other models as seen in Table 4.2. This highlights the influence of assumed boundary conditions on FEA results and ultimate capacity in general. This boundary condition effect is validated by the conservative values for ultimate capacity estimated using empirical methods.

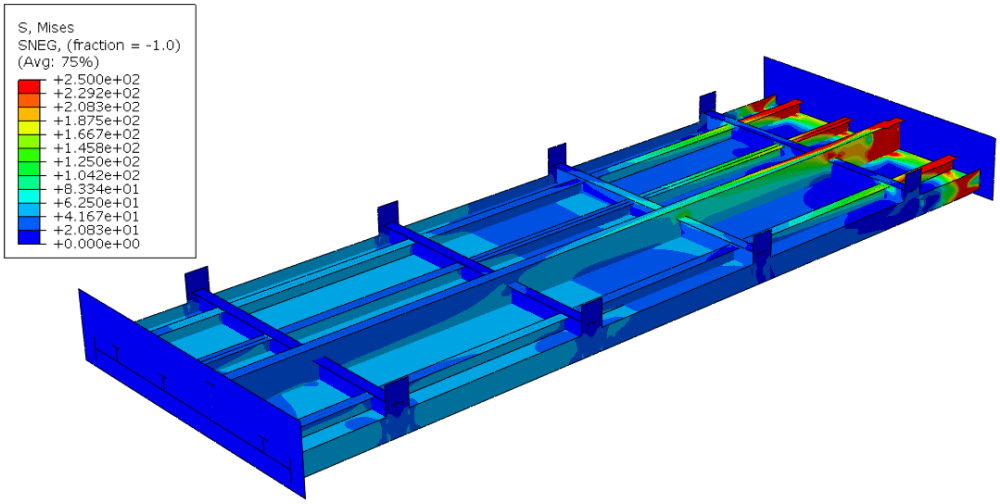

Figure 4.15: Model (BM4) behaviour for a boundary condition with free displacement and rotation

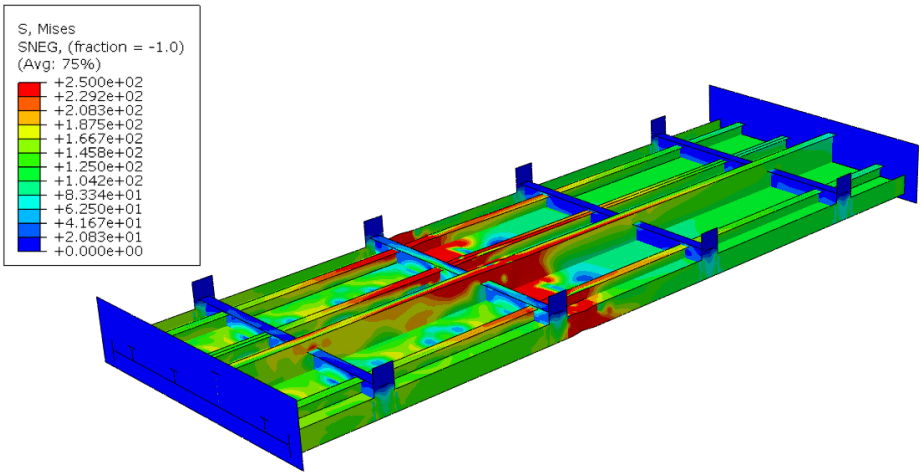

Figure 4.16: BM1 response to general static analysis

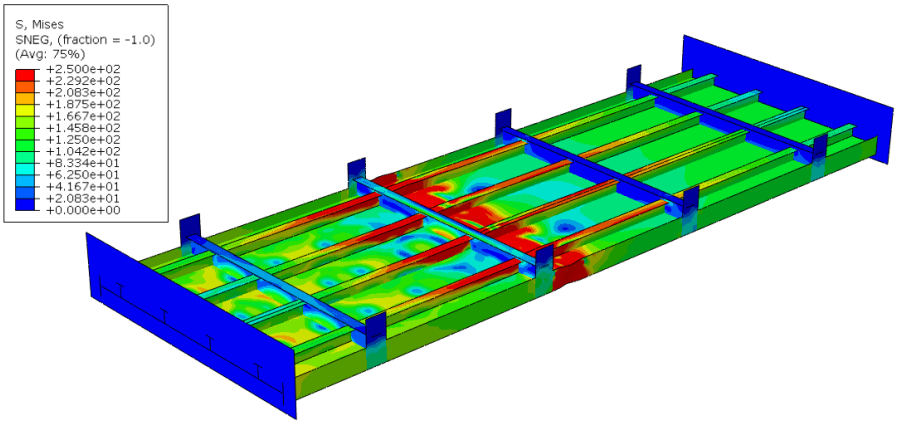

Figure 4.17: LS1 response to general static analysis

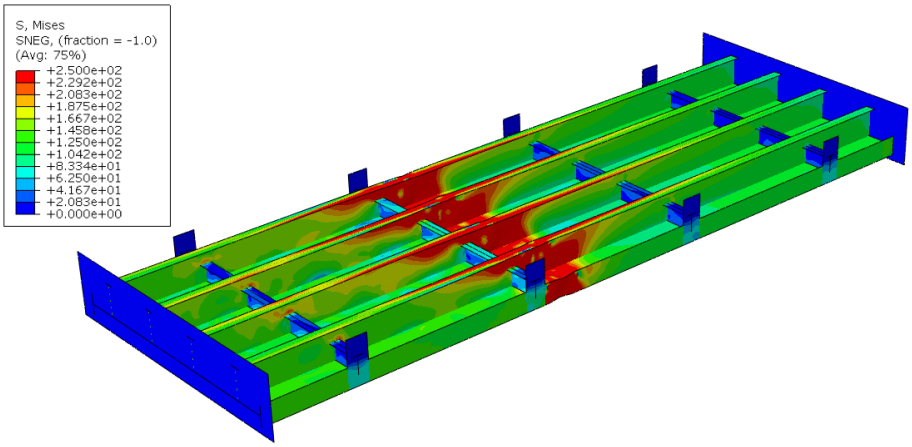

Figure 4.18: LG1 response to general static analysis

Looking at Figure 4.17 and Figure 4.18 above, the changes made to the base model do not change the location of failure. The geometry has been significantly altered in both cases but failure is still recorded in the same section as Figure 4.16 (BM1). However, in Figure 4.19 below there is a slight shift in the location of failure. Failure occurs at the middle of the bottom plate for a uniform plate field. This is consistent with the results from linear buckling analysis and corresponds with the buckling shape in Figure 4.2.

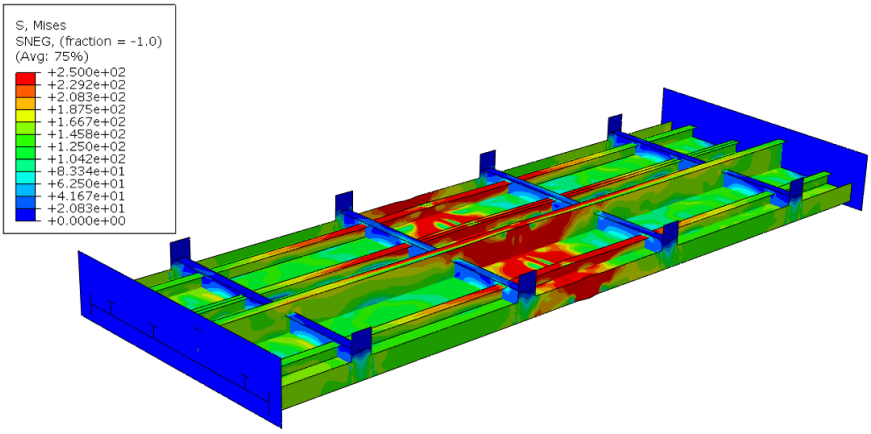

Figure 4.19: BM2 response to general static analysis

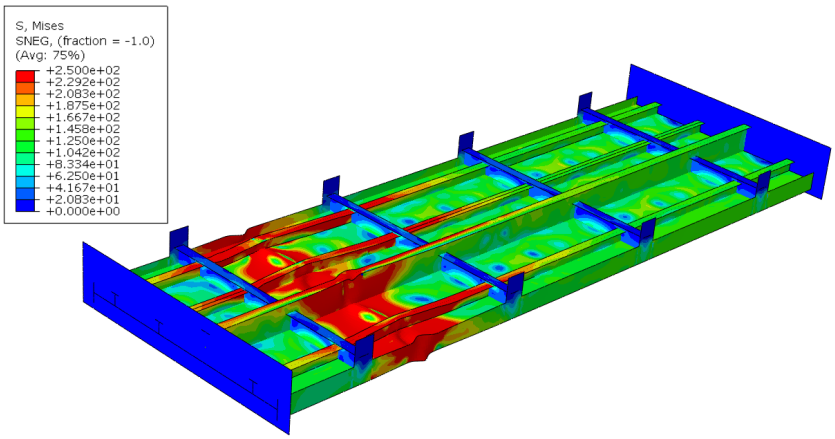

Figure 4.20: BM5 response to general static analysis

No agreement between the reference experiment, reference study and this thesis on the location of failure for most of the models studied. The model (BM5) with a uniform bottom plate thickness of 6.35mm predicted failure in the same section as the reference experiment as seen in Figure 4.20. The collapse mechanism recorded for this model (BM5) appears to compare favorably to the eigenvalue buckling shape recorded for models with a varying bottom plate field Figure 4.1.

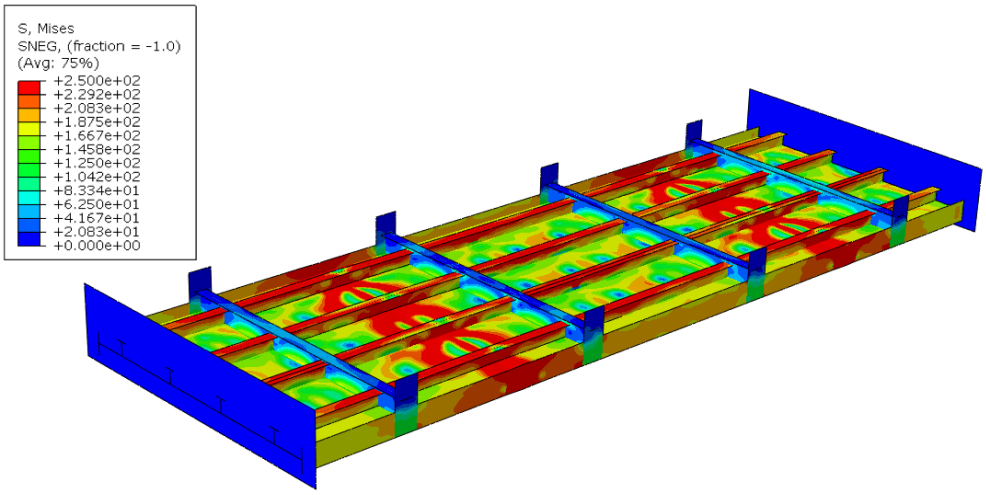

Figure 4.21: LS3 response to general static analysis

Analysis of a model with longitudinal stiffeners and bottom plate thickness of 6.35 mm collapses in the manner shown in Figure 4.21. The mechanism of failure in this model is consistent with the buckling shape for models with uniform bottom plate fields Figure 4.2.

The ultimate capacity estimated by the reference study is in agreement with that estimated in this thesis. This validates the modelling methods employed for this study. This thesis has however investigated a number of reasons for this discrepancy and provided some useful insight. By modifying the base model (BM1) and subjecting the resultant models to non-linear finite element analysis, the parameter that influences the failure of the structure has been investigated systematically.

4.5 Discussion

As mentioned in section (2.5), the reference study by Ringsberg et al. (2021) was done in phases. Additional details such as measured imperfections, residual stresses and true stress-strain were introduced as the study progressed. These additional data improved the ultimate capacity prediction and influenced the failure location. The focus of this thesis however is one phase 1 of the study where nominal properties are used for analysis.The study showed that the niminal material properties were able to predict an acceptable value for ultimate capacity. This value although conservative was deemed sufficient for phase 1 of the study. The measured imperfection, residual stress and true stress – strain data have therefore not been accounted for in this thesis. The ultimate capacity recorded in the BM1 model (4.97 MN) was therefore expected to be conservative when copared to those from the reference experiment (6.59 MN) and phase 3 – 3 (6.22 MN) of the study. The ultimate capacity for the BM1 model is however in agreement with mean ultimate capacity value from phase 1 (4.93 MN) of the study.

With respect to material model, the earlier phases of the study recorded a large scatter in predicted ultimate capacity as a result of the constitutive material model selected. The multilinear (ML) behaved diffently from the bilinear (BL) and elastic – plastic (EP) material models. ML material models presented lower ultimate capacity values. As ML and BL modelss have not been studied in this thesis, their influence on the ultimate capacity for the models studied have not been investigated.

The non-linear FEAs carried out on modified geometries highlight the role of modelling practices and implementation of imperfection in the analysis of stiffened panel structures. It also reveals the limitations of FEA for a stiffened panel. The stiffeners are attached to the bottom plate field by welds and cracks may appear in these welds during loading. FEA would therefore be unable to account for these possible cracks and would therefore not have a 100% agreement with the reference experiment. This was however not the case for this experiment and no emphasis has been placed on crack formation in the joints and welds for this study.

5 Conclusions

The analytical estimation of critical buckling stresses for simplified panel geometry was achieved by implementing established empirical models. The factors affecting ultimate strength capacity were studied both analytically and by running non-linear FEA.

The calculation of ultimate capacity for simplified panel geometry using empirical formula provided the unique opportunity to investigate the factors affecting ultimate capacity. The factors considered were sensitive to the thicknesses of the bottom plate field and stiffener dimensions. These were chosen after a study of some existing formulations for for ultimate capacity. The empirical formula mentioned all stem from two key parameters (plate and column slenderness ratios). These parameters are derivatives of bottom plate and stiffener web thicknesses. A variation of these parameters therefore provided insight into their interaction to influence the ultimate capacity of a stiffened plate structure.

The modifications made, and subsequent models created and analyzed allowed for the study of structural components that make up the plate structure. The thesis studied the influence of these components on the ultimate capacity and post-buckling behaviour of a given model. The studied models where the bottom plate field was made uniform showed an increased stiffness provided by plate uniformity. Models with varying stiffener dimensions showed that the stiffness was influenced by the web height. Failure in a variant of these models where a girder was left in place was governed by the girder.

From these results, it was therefore concluded that model complexity influences the predicted results by introducing uncertainties. These complexities include the varied plate thicknesses of the bottom plate field, the stiffener configuration and the presence of welded joints. By simplifying the base model, the effects of the stiffener and plate dimensions were been investigated.

The load-bearing capacity of the structure is significantly increased by applying a uniform plate thickness of 7.94 mm as seen in BM2 with an ultimate capacity of 6.05 MN. The capacity is however diminished by a reduced plate thickness 6.35 mm as seen in BM5 with an ultimate capacity of 5.08 MN. This uniformity in plate thickness influences the location of failure more so in BM5 and LS3 models. The location of failure recorded in the BM5 model is consistent with the failure location from the reference experiment. There is also some agreement in failure location between the reference experiment and the LS3 model. It can therefore be concluded that the thickness of the bottom plate field came closet to providing insight into the discrepancy in failure location between reference experiment and FEA. This also shows that failure location recorded in the reference experiment was largely governed by the thinner plate of thickness 6.35mm.

It was concluded that the bottom plate field bottom plate field significantly impacts FEA failure results. This is because, of all the modifications made and models created, only the change in plate uniformity and thickness had an effect on the failure location. It was also concluded that the direction of force application, everything else kept constant does not impact the ultimate capacity and location of failure. As mentioned in the reference study, some of the assumptions made regarding the reference experiment may have changed during loading. These changes could have caused something to go wrong in the experiment which is unrecorded and therefore can not be replicated in FE

models. One of the aforementioned assumptions is that of a perfectly rigid boundary. The boundary could have become less rigid during the compression cycle and post buckling phase. The possible effect of diminished rigidity in the boundary conditions prescribed in FE models has been investigated and proved to influence the location of failure recorded.

6 Future work

Further investigation into the interaction between boundary conditions, force direction and geometry modification could prove insightful. Just one of the aforementioned parameters is considered for each of the models, no consideration is given to their possible interaction and influence on failure location.

Nonlinear finite element analysis of model LG3 with modified displacement control >15 mm could be carried out. This would provide insight into the post-buckling behaviour of those models.

7 References

Asariotis, R., Assaf, M., Benamara, H., Hoffmann, J., Premti, A., Rodríguez, L., Weller, M., Youssef, F., Bradford, G., Crowe, T., Davidson, N., Faghfouri, M., Garratt, M., Hutley, S., Konsta, K., de Langen, P., Lehmacher, W., Malby, S., Merk, O., … Visser, D. (2018). Review of Maritime Transport. United Nations Conference on Trade and Development, Geneva, Switzerland, 2018.

Dassault Systèmes Simulia Corp. (2022). Abaqus/CAE 2022. Dassault Systèmes Simulia Corp.

DET NORSKE VERITAS. (2004). NAUTICUS HULL USER MANUAL PULS. www.dnv.com/software

Du, J., Yang, P., Cui, C., & Xia, T. (2015). Ultimate Strength of Steel Panels and Stiffened Plates with Longitudinal Through-thickness Cracks under Compression. 4th International Conference on Sustainable Energy and Environmental Engineering (ICSEEE 2015), Shenzen, China, December 20-21, 2015.

J.K. Paik, S.J. Kim, D.H. Kim, D.C. Kim, P.A. Frieze, M. Abbattista, M. Vallascas, & O.F. Hughes. (2011). Benchmark study on use of ALPS/ULSAP method to determine plate and stiffened plate ultimate strength. Proceedings of MARSTRUCT 2011 Conference, Hamburg, Germany, 28-30 March.

Kim, D. K., Lim, H. L., Kim, M. S., Hwang, O. J., & Park, K. S. (2017). An empirical formulation for predicting the ultimate strength of stiffened panels subjected to longitudinal compression. Ocean Engineering, 140, 270–280. https://doi.org/10.1016/j.oceaneng.2017.05.031

Kim, D. K., Lim, H. L., & Yu, S. Y. (2019). Ultimate strength prediction of T-bar stiffened panel under longitudinal compression by data processing: A refined empirical formulation. Ocean Engineering, 192. https://doi.org/10.1016/j.oceaneng.2019.106522

Lin, Y. T. (1985, March). Ship longitudinal strength modelling. Department of Naval Architecture and Ocean Engineering, University of Glasgow, Scotland, UK.

MAESTRO 11.0.0 2. (2014). ALPS/ULSAP, A Computer Program for Ultimate Limit State Assessment for Stiffened Panels.

Paik, J. K., & Thayamballi, A. K. (1997). An Empirical Formulation For Predicting the Ultimate Compressive Strength of Stiffened Panels. Proceedings of the 7th International Offshore and Polar Engineering Conference, Honolulu, Hawaii, USA, May 25-30 (1997), 328–338.

Paik, J. Kee., & Thayamballi, A. Kumar. (2003). Ultimate limit state design of steel plated structures (S. G. The Atrium, Ed.; First). John Wiley & Sons, Inc.

Ringsberg, J. W., Darie, I., Nahshon, K., Shilling, G., Vaz, M. A., Benson, S., Brubak, L., Feng, G., Fujikubo, M., Gaiotti, M., Hu, Z., Jang, B. S., Paik, J. K., Slagstad, M., Tabri, K., Wang, Y., Wiegard, B., & Yanagihara, D. (2021). The ISSC 2022 committee III.1-Ultimate strength benchmark study on the ultimate limit state analysis of a stiffened plate structure subjected to uniaxial compressive loads. Marine Structures, 79. https://doi.org/10.1016/j.marstruc.2021.103026

Stevens, P. (2018). Extractive Industries: The management of resources as a driver of sustainable development (T. Addison & A. Roe, Eds.). Oxford University Press. https://doi.org/10.1093/oso/9780198817369.001.0001

Zhang, S., & Khan, I. (2009). Buckling and ultimate capability of plates and stiffened panels in axial compression. Marine Structures, 22(4), 791–808. https://doi.org/10.1016/j.marstruc.2009.09.001

8 Appendix

8.1 Simulation matrix

S/N	Task ID	Geometry	Plate thickness	Force location	Force direction	Boundary condition	Material model
1	BM1	stiffener and girder	$t_{1,2}$	EPn	(-x)	clamped	Elastic Perfectly Plastic
2	BM2	stiffener and girder	t_1	Epn	(-x)	clamped	Elastic Perfectly Plastic
3	LS1	longitudinal stiffener	$t_{1,2}$	EPn	(-x)	clamped	Elastic Perfectly Plastic
4	LS2	longitudinal stiffener	t_1	EPn	(-x)	clamped	Elastic Perfectly Plastic
5	LG1	longitudinal girder	$t_{1,2}$	EPn	(-x)	clamped	Elastic Perfectly Plastic
6	LG2	longitudinal girder	t_1	EPn	(-x)	clamped	Elastic Perfectly Plastic
7	LS3	longitudinal stiffener	$t_{1,2}$	EPn	(-x)	free	Elastic Perfectly Plastic
8	LS4	longitudinal stiffener	t_1	EPn	(-x)	free	Elastic Perfectly Plastic
9	LG3	longitudinal girder	$t_{1,2}$	EPn	(-x)	free	Elastic Perfectly Plastic
10	LG4	longitudinal girder	t_1	EPn	(-x)	free	Elastic Perfectly Plastic
11	BM3	stiffener and girder	$t_{1,2}$	EPs	x	clamped	Elastic Perfectly Plastic
12	BM4	stiffener and girder	t_1	EPs	x	clamped	Elastic Perfectly Plastic
13	LS5	longitudinal stiffener	$t_{1,2}$	EPs	x	clamped	Elastic Perfectly Plastic
14	LS6	longitudinal stiffener	t_1	EPs	x	clamped	Elastic Perfectly Plastic
15	LG5	longitudinal girder	$t_{1,2}$	EPs	x	clamped	Elastic Perfectly Plastic

16	LG6	longitudinal girder	t_1	EPs	x	clamped	Elastic Perfectly Plastic
17	LS7	longitudinal stiffener	$t_{1,2}$	EPs	x	free	Elastic Perfectly Plastic
18	LS8	longitudinal stiffener	t_1	EPs	x	free	Elastic Perfectly Plastic
19	LG7	longitudinal girder	$t_{1,2}$	EPs	x	free	Elastic Perfectly Plastic
20	LG8	longitudinal girder	t_1	EPs	x	free	Elastic Perfectly Plastic

8.2 Python code for ultimate strength prediction

```
#ANALYTICAL SOLUTIONS TO ULT STR
#VARIABLES
a = 7315 #mm
b = 610 #mm
tp = 22.95 #mm
hw = 308.86 #mm
tw = 5.97 #mm
bf = 101.73 #mm
tf = 8.89 #mm
sigma_y = 322 #MPa
E = 200000 #MPa
pi = 3.14159265359

#Cofficients for empirical formulation as proposed by (Kim D et al, 2019)
c0 = -0.1449
c1 = 2.9787
c2 = -2.6098
c3 = -0.2418
c4 = 0.0012374
c5 = 0.013470
c6 = 0.8841
c7 = -0.3361
c8 = 0.0015975
c9 = 0.0027745
c10 = -0.0075919
c11 = 0.000032442
c12 = 0.000049670
c13 = -0.013267     #must be negative to correctly predict sigma_u
c14 = -0.000054149

Ap = b*tp
Aw = hw*tw
Af = bf*tf
A = Ap+Aw+Af
z0 = ((Ap*(0.5*tp))+(Aw*(tp+0.5*hw))+(Af*(tp+hw+0.5*tf)))/A
I = ((b*(tp**3))/12)+(Ap*((z0-(tp/2))**2))+(((hw**3)*tw)/12)+(Aw*(tp+(hw/2)-
z0)**2)+((bf*(tf**3))/12)+(Af*(tp+hw+(tf/2)-z0)**2)
r = (I/A)**(1/2)
lamda = (a/(pi*r))*(sigma_y/E)**(1/2)
beta = (b/tp)*(sigma_y/E)**(1/2)
x = hw/tw
y = ((b**3)*tp)/(hw*(tw**3)+(bf**3)*tf)

sigma_u =
((c0+((c1+(c2*(lamda**(1/2)))+(c3/beta)+(c4*x)+(c5*(y**(1/2)))))*(lamda**(1/2)))\

+((c6+(c7/beta)+(c8*x)+(c9*(y**(1/2))))*(1/beta))+((c10+(c11*x)+(c12*(y**(1/2))))
*(x))\
            +((c13+(c14*(y**(1/2))))*(y**(1/2))))
```

DEPARTMENT OF MECHANICS AND MARITME SCIENCES
CHALMERS UNIVERSITY OF TECHNOLOGY
Gothenburg, Sweden 2022
www.chalmers.se

CHALMERS
UNIVERSITY OF TECHNOLOGY